Modeling of gas generation from the Cameo coal zone in the Piceance Basin, Colorado

Etuan Zhang, Ronald J. Hill, Barry J. Katz, and Yongchun Tang

ABSTRACT

The gas generative potential of the Cretaceous Cameo coal in the Piceance Basin, northwestern Colorado, was evaluated quantitatively by sealed gold tube pyrolysis. The H/C and O/C elemental ratios show that pyrolyzed Cameo coal samples follow the Van Krevelen humic coal evolution pathway, reasonably simulating natural coal maturation. Kinetic parameters (activation energy and frequency factor) for gas generation and vitrinite reflectance (R_o) changes were calculated from pyrolysis data. Experimental R_o results from this study are not adequately predicted by published R_o kinetics and indicate the necessity of deriving basin-specific kinetic parameters when building predictive basin models.

Using derived kinetics for R_o evolution and gas generation, basin modeling was completed for 57 wells across the Piceance Basin, which enabled the mapping of coal-rank and coalbed gas potential. Quantities of methane generated at approximately 1.2% R_o are about 300 standard cubic feet per ton (scf/ton) and more than 2500 scf/ton (in-situ dry-ash-free coal) at R_o values reaching 1.9%. Gases generated in both low- and high-maturity coals are less wet, whereas the wetter gas is expected where R_o is approximately 1.4–1.5%. As controlled by regional coal rank and net coal thickness, the largest in-place coalbed gas resources are located in the central part of the basin, where predicted volumes exceed 150 bcf/mi^2, excluding gases in tight sands.

INTRODUCTION

Tight gas sandstones in the Upper Cretaceous Williams Fork Formation in the Piceance Basin in northwestern Colorado,

Manuscript received February 1, 2006; provisional acceptance May 1, 2006; revised manuscript received August 30, 2007; final acceptance April 2, 2008.
DOI:10.1306/04020806015

AUTHORS

ETUAN ZHANG ~ *Shell Exploration and Production Company, BTC, P.O. Box 481, Houston, Texas 77001; etuan.zhang@shell.com*

Etuan Zhang received his Ph.D. from Pennsylvania State University. He has more than 14 years of industrial experience in petroleum exploration and production research. His research interests include petroleum system analysis, basin modeling, source rock pyrolysis and reaction kinetics, and investigation of unconventional resources.

RONALD J. HILL ~ *Geology Program, Western State College, Gunnison, Colorado, 81230; rhill@western.edu*

Ronald Hill specializes in petroleum geochemistry and has more than 12 years of oil industrial and government experience. Currently, he occupies the Moncrief Chair in Petroleum Geology at Western State College in Gunnison, Colorado. His research interests include shale-gas resources and processes that control petroleum generation. Ron holds geology degrees from Michigan State University (B.S. degree) and the University of California, Los Angeles (Ph.D.), and a geochemistry degree from the Colorado School of Mines (M.S. degree).

BARRY J. KATZ ~ *Chevron Corporation, Energy Technology Company, Houston, Texas 77002; barrykatz@chevron.com*

Barry Jay Katz received his B.S. degree in geology from Brooklyn College and his Ph.D. in marine geology and geophysics from the University of Miami. He has held various technical and supervisory positions in Texaco's, ChevronTexaco's, and Chevron's technology organizations since joining Texaco in 1979. Barry is currently a Chevron Fellow and team leader for the hydrocarbon charge in Chevron's Energy Technology Company.

YONGCHUN TANG ~ *Petroleum Energy and Environment Research Center, California Institute of Technology, Covina, California 91722; tang@peer.caltech.edu*

Prior to joining the California Institute of Technology, Tang had more than 15 years of industrial experience in both upstream and downstream research at Chevron. He is currently

the director for the Petroleum Energy and Environment Research Center at the California Institute of Technology. Tang has published more than 80 articles in the field of geochemistry, chemistry, and petroleum engineering. His major research interests are applying molecular modeling and experimental simulation techniques to energy-related problems. He has pioneered the molecular modeling technique to many fields of organic geochemistry, surface chemistry, reaction kinetics, and other petroleum chemistry fields. Tang feels that the major technical barrier of molecular modeling for the petroleum industry is the lack of integration between theory and experiments. Thus, his research group has a strong integration of modeling and experimental efforts. His main research focuses are (1) modeling both homogenous and heterogeneous catalysis; (2) geochemical modeling; (3) interfacial phenomenon modeling (liquid-liquid, liquid-solid, and gas-solid); (4) the nucleation process; (5) emulsion; and (6) ionic liquids.

ACKNOWLEDGEMENTS

We acknowledge the support of Chevron Corporation and Shell Exploration and Production Company, and express our appreciation for their approval to publish the results of our study. We also wish to thank Ron Johnson, Vito Nuccio, Adry Bissada, Jack C. Pashin, Jerry J. Sweeney, and Peter D. Warwick for constructive reviews that significantly improved the article.

western United States (Figure 1), contain some of the largest unconventional gas resources in the Rocky Mountain region. Preliminary reserve estimates indicate 322 tcf of gas in place (GIP) (Johnson et al., 1987). They are thought to be sourced mostly from the Cameo coal zone in the lower part of the Cretaceous Williams Fork Formation. Much of these resources are mostly thermogenic in origin based on the gas carbon isotopic compositions (Johnson and Rice, 1990), although bacterial methanogenesis is thought to be common in many coalbed methane reservoirs (Scott et al., 1994; Pitman et al., 2003) and should contribute to the resource base in the Williams Fork Formation.

Whereas attention to resources in tight gas sands in the Piceance Basin is quite high, interest in the Cameo and other coals in the western United States as both reservoirs and sources for natural gas has recently increased. To better assess the coalbed gas potential of the Cameo coal and to minimize exploration risk, systematic analyses of the gas content and sorption capacity of the coal are certainly important (Eddy et al., 1982; Tyler et al., 1996), but so is the quantitative evaluation of the basinwide thermogenic gas generation potential of the coal.

The timing and extent of thermogenic hydrocarbon generation by a coal-bearing source rock interval depend on both the burial or thermal history and the reaction kinetics of hydrocarbon generation. A variety of physical and chemical methods have been used for the evaluation of organic-matter thermal maturity and for the interpretation of coal and source rock thermal history, with vitrinite reflectance (R_o) as the most widely used tool (Hunt, 1979; Waples, 1981; Tissot and Welte, 1984; Bustin, 1987; Lerche, 1990; Zhao and Lerche, 1993). However, the validity of using R_o to indicate organic maturity and to interpret the thermal history in a sedimentary basin depends on how well the kinetics of vitrinite maturation is understood. Several published R_o kinetic models that purport to be globally applicable exist; however, they consistently fail to perform in some areas of the world (Buiskool Toxopeus, 1983; Ungerer, 1990; Throndsen et al., 1993; Tang et al., 1996). This underscores the need for the development of basin-specific R_o kinetic models.

From the standpoint of exploration and basin modeling, it is also important to know the timing and quantities of methane and other hydrocarbon and nonhydrocarbon gases generated during maturation. Previous studies (Juntgen and Karweil, 1966a, b; Higg, 1986; Burnham and Sweeney, 1989; Tang et al., 1996) attempted to quantitatively evaluate the generation of coalbed gas using two basic approaches: laboratory pyrolysis and theoretical mass balance. All these approaches have much

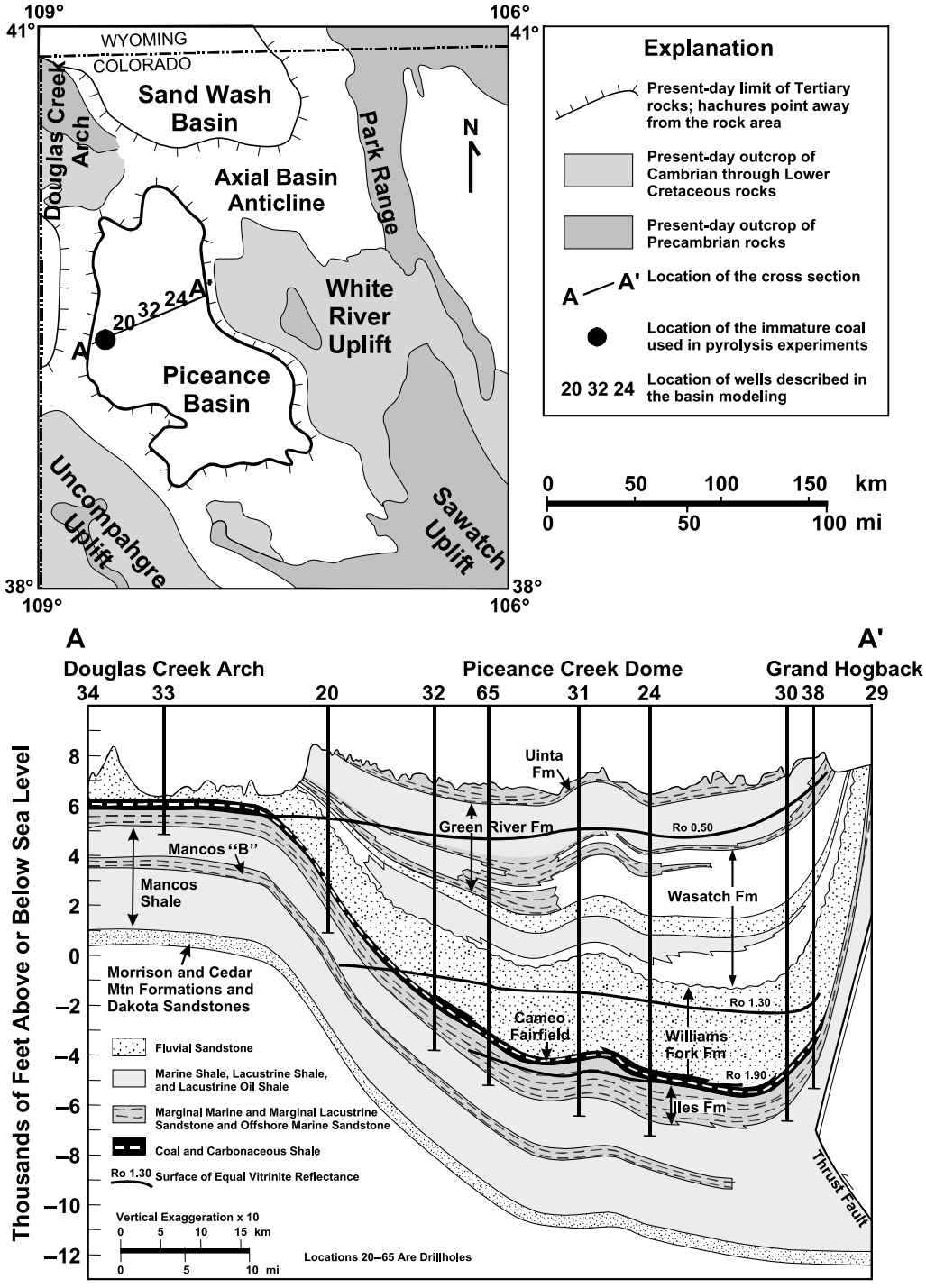

Figure 1. Locations of the Piceance Basin and surrounding geologic features in northwestern Colorado and an east–west cross section (AA′) across the central part of the basin showing the stratigraphic positions of three R_o (%) levels. The cross section is modified from Johnson and Rice (1990). Numbered wells are listed in Table 5.

uncertainty associated with them. The Juntgen and Karweil (1966a, b) elemental mass balance model ignored the production of water during coalification and thus overestimated the amount of methane generated. The Higg (1986) model predicted methane generation directly from pyrolysis data, but the pyrolysis experiments were conducted at an initial pressure of 1 bar. Under high pressures, typical of geological environments, the rate of methane generation may be significantly different from that observed under low-pressure conditions (Hill et al., 1994). The Burnham and Sweeney (1989)

model used gas generation kinetics derived from open-system pyrolysis experiments; however, low pressures and high temperatures may change the dominant chemical-reaction mechanisms occurring during hydrocarbon generation. Furthermore, an open-system pyrolysis of coal typically generates large amounts of light hydrocarbon gases, hydrocarbon liquids, and tar. The cracking of these components to gas and insoluble organic residue occurs during natural coalification but is not accounted for in an open-system model. Tang et al. (1996) conducted a kinetic study of a North Dakota lignite using the sealed gold tube pyrolysis technique. From their specific kinetic models for vitrinite maturation and gas generation, they were able to predict the economic threshold of methane generation relative to organic maturation. However, their kinetic model was derived for a coal rank with an R_o less than 1.5% and thus can be used only for the prediction of relatively early methane generation but not late generation, which occurs at an R_o greater than 1.5%.

Although published data provide a general understanding of coalbed gas generation relative to coal rank and composition, many questions still exist concerning how best to predict the size of coalbed methane accumulations from specific coal units. Organic maturation and hydrocarbon generation are kinetically controlled processes, so the integration of basin modeling with the kinetics of source rock maturation and hydrocarbon generation provides the means by which the thermal maturation and gas generation potentials of the source rocks are numerically formulated. Because the quantitative assessment of the coalbed methane gas potential is critical, we conducted a basin modeling of the gas generation from the Cameo coal zone in the Piceance Basin. The primary objectives of this study were to (1) develop a set of specific kinetic models for gas generation and R_o evolution for the Cameo coal zone, (2) reconstruct the burial and thermal history of the coal measures, and (3) predict the quantity and composition of the generated gas. The scope of the study includes (1) collecting a representative sample of the Cameo coal that is only marginally mature for gas generation as a starting material for pyrolysis tests, (2) conducting sealed gold tube pyrolysis at two heating rates and elevated pressure, (3) developing the specific kinetics parameters for gas generation and R_o evolution, (4) basin modeling on 57 wells across the Piceance Basin for mapping coal-rank patterns and coalbed gas potentials, and (5) comparing the gas generation potential with the gas adsorption capacity of the Cameo coal determined by Eddy et al. (1982) and Tyler et al. (1996) to estimate gas migration into other reservoirs. This article documents the results of the study and discusses the exploration and exploitation significance of the models we derived.

Geological Setting

The Piceance Basin in northwestern Colorado is an intermontane basin formed during the Late Cretaceous through Eocene Laramide orogeny (Greis, 1983; Johnson and Nuccio, 1986). The basin is bounded by the Axial Basin arch to the north, White River uplift to the east, Sawatch uplift to the southeast, Uncompahgre uplift to the southwest, and Douglas Creek arch to the west (Figure 1). The basin is elongated northwest–southeast and occupies approximately 7200 mi^2 (18,648 km^2) (Tremain and Toomey, 1983). The Piceance Basin has gently dipping flanks on the west and southwest and a steep flank on the east; the structural axis trends northwest near the east basin margin (Figure 1) (Greis, 1983; Johnson and Nuccio, 1986). The stratigraphic sequence in the basin (Figure 1) includes (1) the Upper Cretaceous Mancos Shale and Mesaverde Group composed in ascending order of the Iles and Williams Fork formations, and (2) the Tertiary Wasatch (Paleocene–Eocene), Green River (Eocene), and Uinta formations (Eocene). The extensive coal deposits near the base of the Williams Fork are believed to be the major source of the large gas resources in the tight sandstone reservoirs of that formation. The gas geochemistry in the basin is summarized by Johnson and Rice (1990).

The Cameo coals throughout the Piceance Basin range in net thickness from 20 to 80 ft (6–24 m) (Johnson, 1989a), with an average thickness of about 50 ft (15 m). The total coal resource is estimated at 380 billion tons (Choate et al., 1984).

The coals are generally low in sulfur content and were interpreted by Collins (1976) to be deposited under freshwater conditions, although he observed high-sulfur coals, indicating brackish origin, at two localities in the southeastern part of the basin. The coal rank near the base of the Cameo coal zone varies from subbituminous A and high-volatile C around the west and southwest basin margins to semianthracite along the structural axis (Johnson and Nuccio, 1986).

METHODS

Unpyrolyzed Coal Sample

The coal sample used in the pyrolysis experiments was collected from the Cameo seam of the Upper Cretaceous Mesaverde Group in the Twin Arrow 4-14 C&K well, which is located in the northwestern Piceance Basin, in Rio Blanco County, Colorado (well 33 in cross section AA′, Figure 1). The initial coal elemental composition is 77 wt.% C, 6 wt.% H, and 14 wt.% O with less than 3 wt.% N and S. The maceral data for the coal sample are summarized in Table 1. This sample is relatively immature with an R_o of 0.5% and a 0.9 H/C atomic ratio. The maceral composition is 87.2% vitrinite, 4.6% liptinite, and 8.2% inertinite, which is petrographically similar to that reported by Law et al. (1989) and also close in petrographic composition to regional coals as reported by Collins (1976). Therefore, it is possible to use the results from the pyrolysis of this coal to model thermogenic gas generation and vitrinite maturation throughout the basin.

Closed-System Pyrolysis

Sealed gold tube pyrolysis experiments were performed on the immature Cameo coal sample from the Twin Arrow 4-14 C&K well under elevated pressure and two heating rate conditions, following the methods of Tang et al. (1996). These experiments allowed us to make mass balance calculations and accurately monitor the changes in gas yield, gas molecular and isotopic compositions, R_o, and elemental composition of the residual coals during maturation.

Table 1. Maceral Analysis of the Cameo Coal Sample from the Twin Arrow 4-14 C&K Well Used in Pyrolysis Experiments

Maceral Composition (vol.%)		
Vitrinite	Liptinite	Inertinite
87.2	4.6	8.2

Pyrolysis experiments were performed using sealed gold tubes (50-mm [1.9-in.] length, 3.6-mm [0.14-in.] inner diameter, and 0.4-mm [0.015-in.] wall thickness) in a high-pressure and high-temperature pyrolysis system developed at Chevron Petroleum Technology Company. The clean tubes were welded at one end before sample loading. About 100 mg of finely powdered, homogenized, vacuum-dried, and gas-free raw coal sample was loaded into each of the duplicate gold tubes in a glove box containing an argon atmosphere. The tubes were flushed with argon in the box for 15 min to insure the complete removal of air. The other end of the gold tube was then welded under an argon atmosphere using the methods of Hill et al. (1994, 1996).

The sealed gold tubes were placed into stainless steel vessels that were then placed in a large oven and kept at a constant pressure of 5000 psi during the course of the experiment. Water was the pressure medium and was controlled by an air-driven pump. The samples were heated using two different nonisothermal heating programs of 10°C/hr from 100 to 490°C and 1°C/hr from 100 to 450°C, respectively. The temperature was controlled using a built-in temperature controller and measured directly with an accuracy of ±1°C with two thermocouples fixed on the top and bottom of each vessel and recorded and stored on the computer. A vessel containing gold tubes was removed from the oven at temperature intervals of 20–30°C between 280 and 490°C. The vessel was quickly cooled to room temperature and then depressurized slowly before the gold tubes were unloaded from the vessels.

Pyrolysis Product Analysis

Pyrolysis products were analyzed for gas yield and molecular composition, as well as for R_o and elemental composition of the residual coal. The analysis began with the collection of gaseous products in a vacuum line (Hill et al., 1994, 1996). In this setup, the gold tube was pierced with a needle in the high vacuum line at room temperature, allowing all the generated gases to be desorbed from the coal sample into the line and the liquid products (C_{6+} fractions) to be captured cryogenically into a dry ice or acetone trap ($T = -77°C$). The gases were collected by a Toepler pump into a calibrated volume for total gas volume quantification and then introduced directly into a gas chromatograph for composition analysis.

The residual coal after gas analysis was subjected to R_o measurements (random R_o). Fifty readings were generally taken on each specimen. The standard deviations for the arithmetic means were 0.05–0.09%. The R_o data provided a measure of the organic maturity of the coal during the pyrolysis experiments. The R_o values of the residue after the pyrolysis were crossplotted against the pyrolysis yields from different heating rates such that the pyrolysis yields obtained at the different heating rates would fall onto roughly a single curve for a given gas product.

The elemental composition (C, H, O, N, and S) of the residual coal was determined by ultimate analysis. All values were determined directly and reported on a dry, ash-free basis.

Kinetics Analysis

Organic matter or coal undergoes thermal cracking to generate hydrocarbons at rates dependent on temperature. The rate of organic matter maturation can be expressed by the first-order kinetic reaction:

$$\frac{dC}{dt} = -kC \qquad (1)$$

where C is the fraction of coal still transformable (unreacted) into hydrocarbons, t is time, and k is the rate constant following the Arrhenius law, i.e., k varies with temperature according to

$$k = Ae^{\frac{-E}{RT(t)}} \qquad (2)$$

where A is the frequency factor (s^{-1}), e is the mathematical constant (= 2.7183) while e^x is the exponential function ($x = -E/RT(t)$), E is the activation energy (kcal/mol), R is the gas constant (= 0.001987 kcal/mol/K), and T is the absolute temperature, which is a function of time (t).

Because coal is a heterogeneous organic material consisting of varying macerals with mostly macromolecular structures and several different types of chemical bonds, its decomposition cannot be described adequately by a single chemical reaction. The kinetic model commonly used for coal thermal decomposition is based on several parallel first-order reactions, with a distribution of activation energies, all occurring simultaneously but independently of each other (Tissot and Welte, 1984; Burnham et al., 1987, 1988; Quigely et al., 1987; Tissot et al., 1987; Espitalie et al., 1988; Burnham and Sweeney, 1989; Ungerer, 1990; Sundararaman et al., 1992; Tang et al., 1996). In this study, the pre-exponential factor and activation energies were derived from the above standard kinetics analysis procedures by fitting the calculated values to values from the pyrolysis data.

Kinetics of Gas Generation

Based on the kinetic approach mentioned above, hypothetical kinetic parameters for the generation of methane, ethane, C_3–C_5, and CO_2 were determined. These were tested against pyrolysis data using the cumulative yields of methane, ethane, C_3–C_5, and CO_2 with increasing temperature and time. The focus of this study is to evaluate the primary gas generation from coal. Thus, pyrolysis reactions were not conducted to completion but were limited to maximum experimental thermal stress equivalent to approximately 2.2% R_o so as to limit the influence of secondary cracking reactions (Behar et al., 1992, 1997). Furthermore, to restrict the range of possible kinetic solutions, two sets of pyrolysis data, obtained at two significantly different heating rates, were used instead of a single heating-rate data

set. Only those solutions that best fit the measured data and have the smallest fitting deviation were accepted for deducing the kinetic parameters. Two uncertainties are involved in the calculation, the uncertainty of the maximum yield and the potentially nonunique kinetic solution based on the two heating rate experiments. Sensitivity analyses for these two uncertainties are discussed below.

Uncertainty of Maximum Gas Yield for Kinetic Fitting

Much work has been done to investigate different methods of deriving kinetics for a closed-system pyrolysis (for example, Tang et al., 1996, and their references). Although gold tubes can be heated to a very high temperature, thereby obtaining an experimentally measured maximum gas yield from a closed-system pyrolysis, this number represents gas generated from primary cracking of coal plus gas generated from secondary cracking of oil from coal, and will bias the pyrolysis maximum gas yield toward products of secondary cracking (Behar et al., 1992, 1997). In an open-system pyrolysis, however, the maximum primary gas yield is measured, but in this case, the yield is very low and cannot be reasonably extrapolated to geological conditions. From our closed-system experimental data, we estimated the maximum gas yield at three levels: gas yield + 50% of gas yield (4800 standard cubic feet per ton [scf/ton]), gas yield + 67% of gas yield (5760 scf/ton), and gas yield + 100% of gas yield (6400 scf/ton). In a summary of a previous work, Tang et al. (1996) estimated the maximum methane yield from coal to be between approximately 4000 and 5760 scf/ton at 3.0% R_o. Except for the gas yield + 100% estimate, our estimates of maximum gas yields fall within that range and provide a basis for evaluating the effect of maximum gas yield on the uncertainty in kinetics analysis.

Uncertainty of Kinetic Fittings

Typically, we performed a sensitivity analysis to evaluate the applicability of the laboratory data to geological field observations. Figure 2 shows the sum of the total errors between the experimental data and calculated results using an optimization program. To decrease the uncertainty of the curve fittings (i.e., getting a unique solution of the frequency factors), increasing either the range or the number of heating rates is required. However, increasing the number of heating rates without increasing the range of heating rates may not significantly reduce the uncertainty. Based on field data and experience from a previous work on coal samples (Chevron internal data), we have followed the methods of Tang et al. (1996) and have adjusted the frequency factor between 10^{11} and 10^{16}/s until the sum of total errors between the experimental and calculated results is minimized.

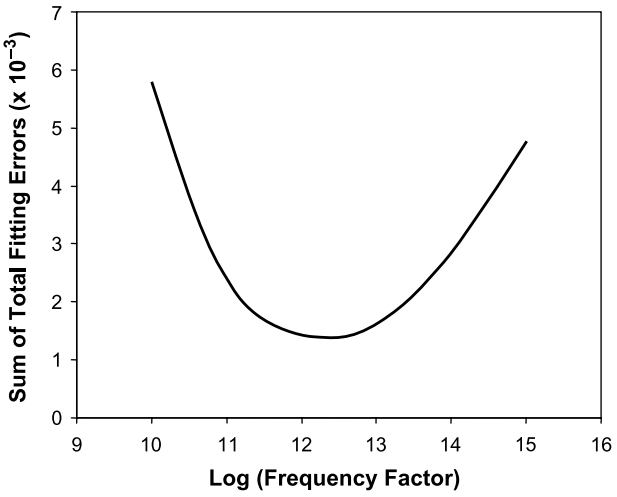

Figure 2. Sum of total errors between the experimental data and calculated results using an optimization program.

Kinetics of Vitrinite Reflectance

For an easier application of the results in this study, we related R_o directly to temperature and time. The basic method for deriving the R_o kinetics employed in the model is similar to that for gas generation kinetics. However, our approach links R_o with the vitrinite conversion index (VCI: 0 to 1). The VCI is defined as

$$\mathrm{VCI} = \frac{(\%\ R_o - 0.2)}{3} \qquad (3)$$

where VCI is in percent, 0.2 is an estimate of the initial R_o that was associated with the material after its initial conversion to vitrinite from the precursor and may represent the zero point for organic thermal maturity, and 3 approaches our maximum point for

organic maturity. The theoretical VCI was calculated using the same chemical kinetic scheme as discussed above. Fitting calculated with measured VCI using experimental R_o and following the VCI-R_o correlation equation (3) allowed us to derive specific kinetic parameters for the R_o evolution of the coal.

Basin Modeling

To evaluate quantitatively the gas generation potential of the Cameo coal, basin modeling was conducted for 57 wells across the Piceance Basin using a one-dimensional (1-D) basin-modeling program, with our gas generation kinetic parameters and R_o evolution kinetics. The modeling inputs included (1) timing and duration of depositional events, thickness and thermal conductivity of the sedimentary sequences including overburden, coal measures, and rocks directly underlying the coal measures; (2) timing and magnitude of erosional events and timing of hiatuses; (3) mean annual surface temperatures and down-hole temperatures; (4) regional heat flow, including heat flow through time; and (5) measured R_o data for the wells from published information and proprietary studies. The models were calibrated against both the present-day geothermics (heat flow consistent with bottom-hole temperatures) and the measured reflectance profile for each well. The study included (1) the reconstruction of burial history using stratigraphic data, (2) the calibration of thermal history based on R_o kinetics and the observed R_o profiles, and (3) the prediction of gas generation by incorporating the gas generation kinetics into the calibrated thermal history models.

Because the Tertiary strata are truncated by the present erosion surface, the original thickness of the Tertiary overburden is unknown. To reconstruct the burial history, the maximum thickness of the removed sediments was estimated indirectly. In this study, an estimate of the maximum depth of burial was made using two approaches: (1) extrapolation of measured "logR_o-depth" plots (Dow, 1977), and (2) thermal modeling adjustment. Assuming that the thermal conductivity of the Tertiary rocks remained constant and that the burial was the dominant heat source affecting the area during coal maturation, exponential reflectance gradients are expected for the sections of maximum burial. With this assumption, logR_o-depth plots were extrapolated to an R_o value of 0.2% to yield the maximum thickness of overburden in each borehole location. The thermal history of a sedimentary basin depends not only on the deposition and erosion history but also on the heat-flow evolution. To estimate the heat-flow history, thermal conductivity and geothermal gradient need to be determined. In this study, the proportions of different lithologies for each formation were calculated using borehole data. An average thermal conductivity for each lithology was used in the modeling as built-in and provided in the basin-modeling program. The present-day geothermal gradient of each borehole location was calculated using down-hole temperatures that were corrected with the aid of mud-log information and Horner plots. As part of the calculation, a mean annual surface temperature of 10°C (Gretener, 1981) was adopted and held constant.

To obtain the thermal history calibration, our model uses the present-day heat flow as one of the input factors. Assuming the burial histories (including amounts of erosion) are correct, the heat flow was adjusted against both observed down-hole temperatures and measured R_o profiles by trial-and-error adjustments until the predicted reflectance profiles best fit the measured profile for each well. Matching the calculated and measured R_o data enabled the burial, temperature, and coal-maturation (R_o) history curves to be obtained for each well.

RESULTS

Vitrinite Reflectance

Variations of R_o for the pyrolysis of the Cameo coal at 10 and 1°C/hr heating rates are reported in Table 2. The R_o values increase from an initial 0.5% to 2.17% (488°C, 10°C/hr) with increasing temperature. This maturity range roughly covers the complete coal-rank series observed for the Cameo coal seams in the Piceance Basin (Nuccio and Johnson, 1983), as well as values spanning the oil and gas windows. Thus, the pyrolysis results can be reasonably used for the kinetic modeling of

Table 2. Vitrinite Reflectance (%R_o) and Elemental Composition Changes with Temperature for the Pyrolysis of the Cameo Coal from the Twin Arrow 4-14 C&K Well, Piceance Basin, Northwestern Colorado

Sample No.	Final Temperature (°C)	R_o(%)	C(%)	H(%)	O(%)	N(%)	S(%)	H/C	O/C	N/C	S/C
1°C/hr											
Raw		0.50	77.03	5.79	14.38	1.87	0.93	0.90	0.14	0.0208	0.0045
25	289	0.81	78.22	5.56	13.34	2.03	0.85	0.85	0.13	0.0222	0.0041
28	317	0.86	79.81	5.73	11.38	2.10	0.97	0.86	0.11	0.0226	0.0046
31	336	1.09	81.45	5.30	10.13	2.21	0.91	0.78	0.09	0.0233	0.0042
18	354	1.33	82.47	5.16	9.21	2.24	0.92	0.75	0.08	0.0233	0.0042
54	370	1.45	84.99	4.90	6.94	2.24	0.94	0.69	0.06	0.0226	0.0041
15	381	1.52	84.30	4.43	7.94	2.36	0.96	0.63	0.07	0.0240	0.0043
23	403	1.74	86.30	4.01	6.46	2.29	0.94	0.56	0.06	0.0227	0.0041
50	420	1.86	88.65	3.73	4.65	2.12	0.87	0.50	0.04	0.0205	0.0037
57	433	1.97	89.38	3.56	4.28	2.05	0.74	0.48	0.04	0.0196	0.0031
55	445	2.09	89.92	3.39	3.86	2.02	0.82	0.45	0.03	0.0192	0.0034
10°C/hr											
98	294	0.66	78.65	5.58	14.19			0.85	0.14		
77	345	0.78	79.97	5.59	11.76			0.84	0.11		
99	380	1.11	81.80	5.27	9.53			0.77	0.09		
72	405	1.36	84.12	4.62	7.79			0.66	0.07		
45	421	1.59	86.03	4.21	6.61			0.59	0.06		
43	435	1.70	87.46	4.00	6.16			0.55	0.05		
30	445	1.83	88.41	3.94	4.17			0.53	0.04		
48	468	2.01	89.16	3.71	3.90			0.50	0.03		
27	488	2.17	89.71	3.49	3.76			0.47	0.03		

vitrinite maturation and hydrocarbon generation to assess coalbed gas potentials for the range of maturities observed in the basin.

Ultimate Analysis

Results of the ultimate analysis conducted on the residual coal as well as on the starting coal sample from the Twin Arrow 4-14 C & K well are given in Table 2. With an increase in simulated maturity, the coal elemental composition changed systematically. Carbon content increased from 77 to 90%, whereas hydrogen and oxygen contents decreased from 6 and 14% down to 3.4 and 3.8%, respectively. Commensurate with the elemental composition changes, the H/C atomic ratio decreased from 0.9 to 0.45, and the O/C atomic ratio decreased from 0.14 to 0.03 with increasing temperature and thermal alteration. When plotted on a Van Krevelen (1993) diagram (Figure 3), these ratios follow an evolution pathway typical for vitrinite-rich coal or type III kerogen.

Sulfur content remained fairly constant (about 0.93%) over the pyrolysis temperature range investigated, except for decreasing at high temperature (>400°C) and maturity (>1.8% R_o) to about 0.7%. The S/C atomic ratio remained roughly constant at 0.0045 from the initial pyrolysis temperature up to 380°C (1°C/hr), above which the ratio decreased to 0.0031.

The N content increased from an initial value of 1.87 to 2.36% for 380°C (1°C/hr) and then decreased to about 2.02% at a temperature of 445°C (1°C/hr). The N/C atomic ratio showed an initial increase from 0.021 to 0.024 at 380°C (1°C/hr) and then decreased to 0.019 when the temperature increased to 445°C. The changes are small and

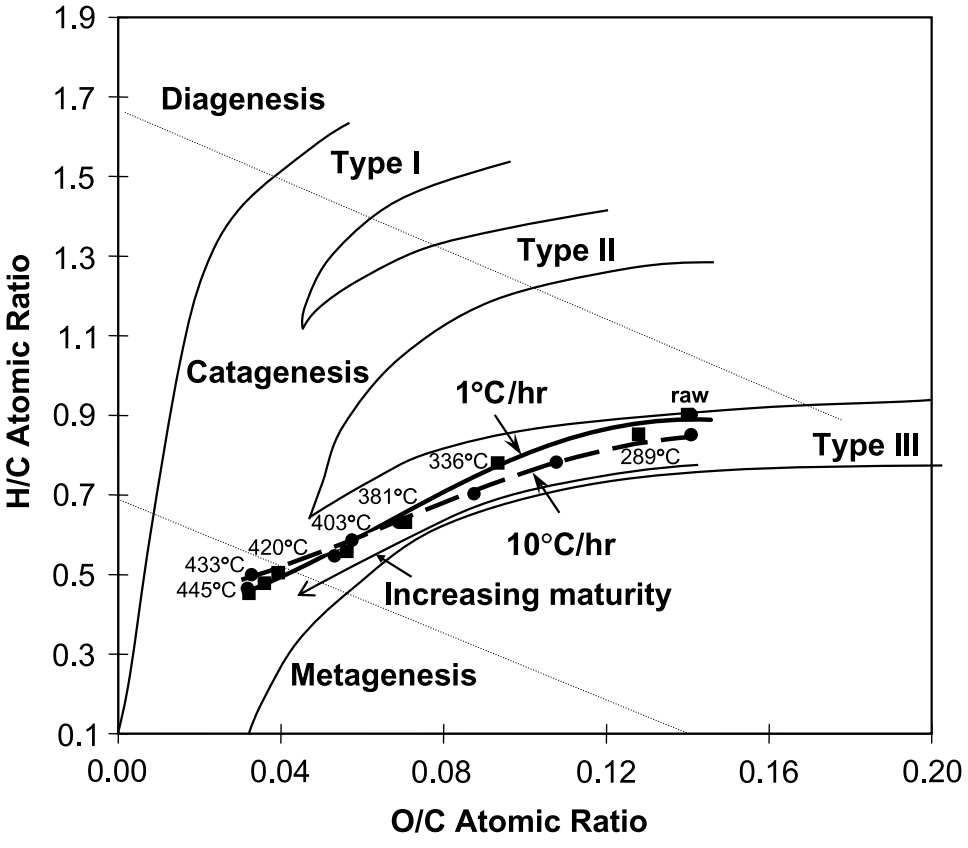

Figure 3. The changes in H/C and O/C atomic ratios for the pyrolysis of the Cameo coal from the Twin Arrow 4-14 C&K well as shown on a Van Krevelen diagram indicate that the simulated maturation of the coal follows the natural evolution trend for type III kerogen. The two faint dotted lines running from about 1.7 and 0.7 on the *y* axis to 0.18 and 0.14 on the *x* axis represent the stage boundaries of organic matter transformation from diagenesis to catagenesis and from catagenesis to metagenesis, respectively.

indicate that both N and S remain in some thermally resistant structures, most likely in N- and S-bearing aromatic structures. Releasing the aliphatic groups during pyrolysis results in the concentration of aromatic structures, causing a decrease in H/C ratios, whereas N and S contents increase relatively, leading to slight increases in both N/C and S/C ratios. At even higher temperatures, the cracking of some aromatic structures occurs, leading to the release of some N and S, so both N/C and S/C ratios decrease with increasing maturity.

According to the Van Krevelen diagram (Figure 3), the positive relation between (1) the increasing R_o and decreasing atomic H/C and O/C ratios and (2) the coal evolution pathway indicates that the sealed gold tube pyrolysis experiments conducted in our study can reasonably simulate the organic maturation observed in nature.

Pyrolysis Gases

Hydrocarbon gases (C_1–C_5) are generated in small amounts at the beginning of the thermal degradation of coal, but they become the dominant gases at high maturity (Table 3; Figure 4). Methane is the major constituent being generated but not in large amounts until temperatures of 380°C at 1°C/hr or 420°C at 10°C/hr are reached. As illustrated in Figures 4 and 5A, the least thermally stressed samples (<300°C, <0.8% R_o) generated only minor amounts of methane, 13 scf/ton of initial dry-ash-free coal (dry-ash-free coal), accounting for only 1.8% of the total generated gas volume. With increasing temperatures up to 380°C (1°C/hr, ≈1.5% R_o), methane yield increased gradually to 580 scf/ton of initial dry-ash-free coal, accounting for about 25% of the total gas volume. As even higher temperatures were applied, a sharper increase in methane yield occurred and rapidly increased to a maximum of 2850 scf/ton of initial dry-ash-free coal in the most altered coal (450°C, 1°C/h, 2.1% R_o). This amount represents 52% or more of the total gas volume.

The C_2–C_5 hydrocarbon yield remained low under low-temperature conditions and then increased exponentially with increasing temperature

Table 3. Gas Composition (scf/ton, Dry-Ash-Free Coal) for the Pyrolysis of the Cameo Coal from the Twin Arrow 4-14 C&K Well

Sample No.	Final Temperature (°C)	R_o(%)	C_1	C_2	C_3	*n*-C_4	*i*-C_4	*n*-C_5	*i*-C_5	Wetness*	CO_2	H_2
1°C/hr												
26	289	0.77	13.0	0.4	0.0	0.0	0.0	0.0	0.0	2.8	367.6	0.4
28	317	0.86	64.7	9.3	2.6	0.4	0.0	0.0	0.0	15.9	590.6	0.4
31	336	1.09	126.0	31.2	13.8	1.9	1.5	0.7	0.4	28.2	962.6	1.1
18	354	1.33	223.0	73.2	35.3	6.3	3.0	1.9	1.9	35.3	1173.7	2.2
20	354	1.32	238.6	82.5	34.9	5.9	2.6	1.5	1.9	35.2	1169.6	2.2
53	370	1.47	370.2	155.7	76.6	17.1	6.3	3.3	5.2	41.7	1351.3	4.1
54	370	1.45	426.7	154.2	75.4	17.1	6.3	3.3	4.8	38.0	1337.6	4.5
15	381	1.52	587.6	194.0	87.7	16.7	8.9	3.3	3.7	34.9	1452.8	7.1
17	381	1.55	569.0	194.0	85.5	15.6	8.5	3.0	3.3	35.3	1457.3	7.1
23	403	1.74	1120.9	301.0	123.0	24.2	14.5	4.8	5.2	29.7	1603.0	12.6
50	420	1.86	1859.0	453.4	181.4	42.4	13.0	3.3	10.4	27.5	1769.1	19.7
49	420	1.91	1821.1	456.0	178.4	40.5	12.6	3.0	9.7	27.8	1769.8	18.6
57	433	1.97	2124.8	483.9	171.0	33.4	10.8	1.9	6.3	25.0	1793.6	28.6
58	433	2.00	2256.3	498.8	175.1	34.9	10.8	1.9	6.7	24.4	1840.5	30.8
55	445	2.09	2725.4	520.7	152.0	20.8	7.4	0.4	1.9	20.5	1864.2	35.7
56	445	2.05	2846.2	527.4	149.8	19.3	7.1	0.4	1.5	19.9	1888.4	40.5
10°C/hr												
12	295	0.68	3.0	0.0	0.0	0.0	0.0	0.0	0.0	0.0	155.0	0.0
6	345	0.83	49.1	4.8	1.1	0.0	0.0	0.0	0.0	10.8	512.9	0.7
11	374	1.05	166.5	47.9	23.4	4.1	2.2	1.5	1.1	32.5	959.6	2.2
4	399	1.36	369.8	126.4	58.7	10.8	10.0	2.2	2.6	36.3	1226.5	5.9
45	421	1.59	631.4	214.1	97.4	22.3	9.3	4.8	6.7	36.0	1397.1	11.5
46	421	1.60	628.5	218.2	99.6	23.0	9.3	4.8	6.7	36.5	1390.0	7.1
43	435	1.70	934.3	293.6	133.1	32.0	13.4	5.9	8.9	34.3	1497.8	21.9
44	435	1.71	968.2	297.3	121.9	27.9	12.6	5.6	7.4	32.8	1538.7	21.2
7	445	1.84	1340.9	369.4	163.9	37.5	17.1	5.2	8.9	31.0	1603.3	20.8
48	468	2.01	1973.1									34.9
47	468	2.00	1964.6	495.4	173.6	33.8	12.6	4.1	5.2	26.9	1745.3	34.6
27	488	2.17	2743.6	527.0	173.2	17.1	9.3	0.4	0.4	21.0	1867.6	53.1

*Wetness = $\sum(C_2 - C_5)/\sum(C_1 - C_5) \times 100$.

(Figure 5B, C). Because the generation rate of C_2–C_5 hydrocarbons is slightly higher than that of methane during this pyrolysis condition, gas wetness ($C_{2-5}/C_{1-5} \times 100$) increased rapidly to a maximum value of 42% at 1.45% R_o (Table 3). Between 1.4 and 1.7% R_o, the gas wetness remains fairly constant. Within this maturity range, the generation rates of both methane and C_2–C_5 hydrocarbons are similar. As temperatures approached 400°C (1°C/hr, ~1.75% R_o), a sharp increase in C_2–C_5 hydrocarbon yield occurred, reaching a maximum yield of 700 scf/ton of initial dry-ash-free coal at 430°C (1°C/hr, ~2% R_o). At temperatures greater than 400°C (1°C/hr), methane generation is faster than that of C_2–C_5 hydrocarbons, leading to a corresponding decrease in gas wetness from that point on. The decrease in gas wetness indicates a significant cracking of the C_2–C_5 hydrocarbons, resulting in a decrease of gas wetness to less than 20% in the most altered coal (450°C, 2.1% R_o).

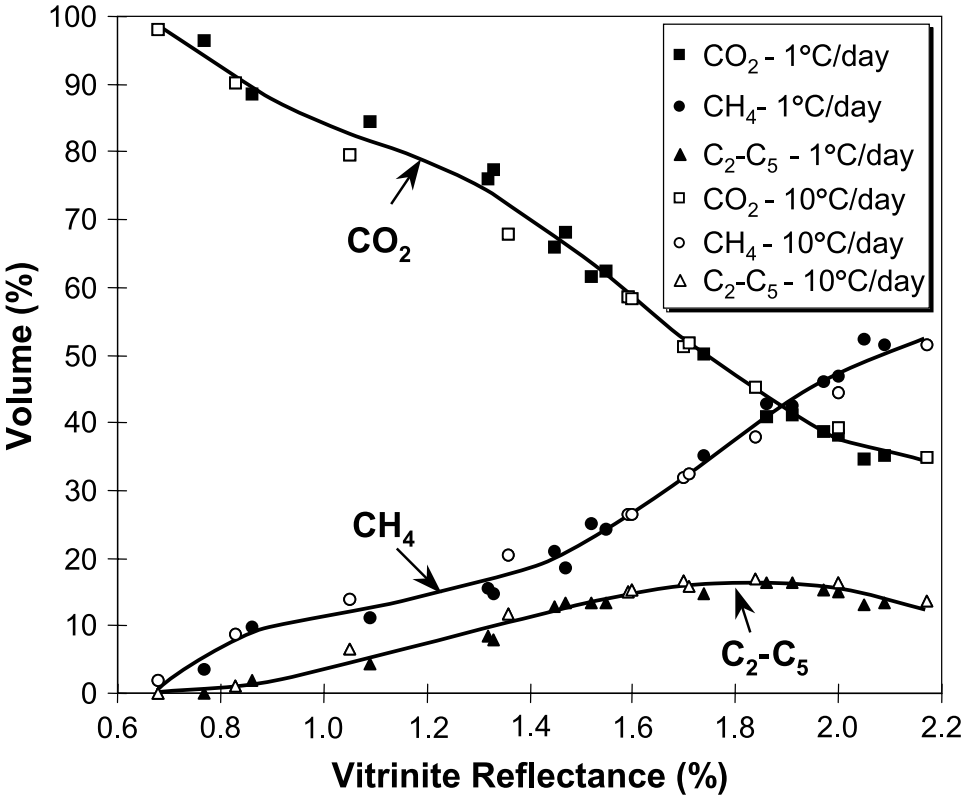

Figure 4. Changes in volume percent of different gases to total gas products versus reflectance values of the residual vitrinite for the pyrolysis of the Cameo coal in the Twin Arrow 4-14 C&K well at 1 and 10°C/hr heating rates.

The dominant nonhydrocarbon gas generated from the Cameo coal is CO_2, and CO_2 was dominant among all gases generated at R_o values to as high as 1.8% (Figure 5d). With increasing temperatures up to 400°C, a gradual but relatively slow increase in the absolute amount of generated CO_2 was observed. Figure 5d plots CO_2 yield versus pyrolysis temperature. Significant CO_2 generation occurred at mild pyrolysis conditions (<340°C). More than 50% of the total CO_2 yield, which accounts for 85% or more of the total gases produced during pyrolysis, was generated at less than 1.1% R_o. This early generation of CO_2 is likely related to the cracking of labile oxygenated functional groups, for instance, decarboxylation of carboxylic groups. This observation is consistent with a relatively fast reduction of O/C atomic ratios during early catagenesis shown on the Van Krevelen diagram (Figure 3).

Kinetics of Gas Generation

In our closed-system pyrolysis of the Cameo coal under various heating rates and durations, methane yields provided the necessary data for calculating the gas generation kinetics parameters for the coal. Table 4 shows the kinetics of gas generation at the three different maximum yields described in the Methods section. Figure 5a–d illustrate the best curve fitting and the kinetic parameter patterns for the generation of methane, ethane, C_3–C_5, and CO_2. Detailed information on the derived kinetic parameters is listed in Table 4. The results show that (1) the generation of methane from the Cameo coal can be described best using a frequency factor (A in equation 2) of $2.218 \times 10^{11}\ s^{-1}$ and activation energies between 43 and 67 kcal/mol (dominant values from 49 to 60 kcal/mol), (2) matching the generation of ethane requires the distribution of activation energies ranging mainly between 53 and 65 kcal/mol with a frequency factor of $6.6753 \times 10^{14}\ s^{-1}$, and (3) the generation of the C_3–C_5 gases requires activation energy values ranging from 58 to 72 kcal/mol with a frequency factor of $2.3364 \times 10^{16}\ s^{-1}$.

The CO_2 generation requires a frequency factor of $4.3693 \times 10^{12}\ s^{-1}$ and activation energies distributed over a range from 43 to 67 kcal/mol, with about

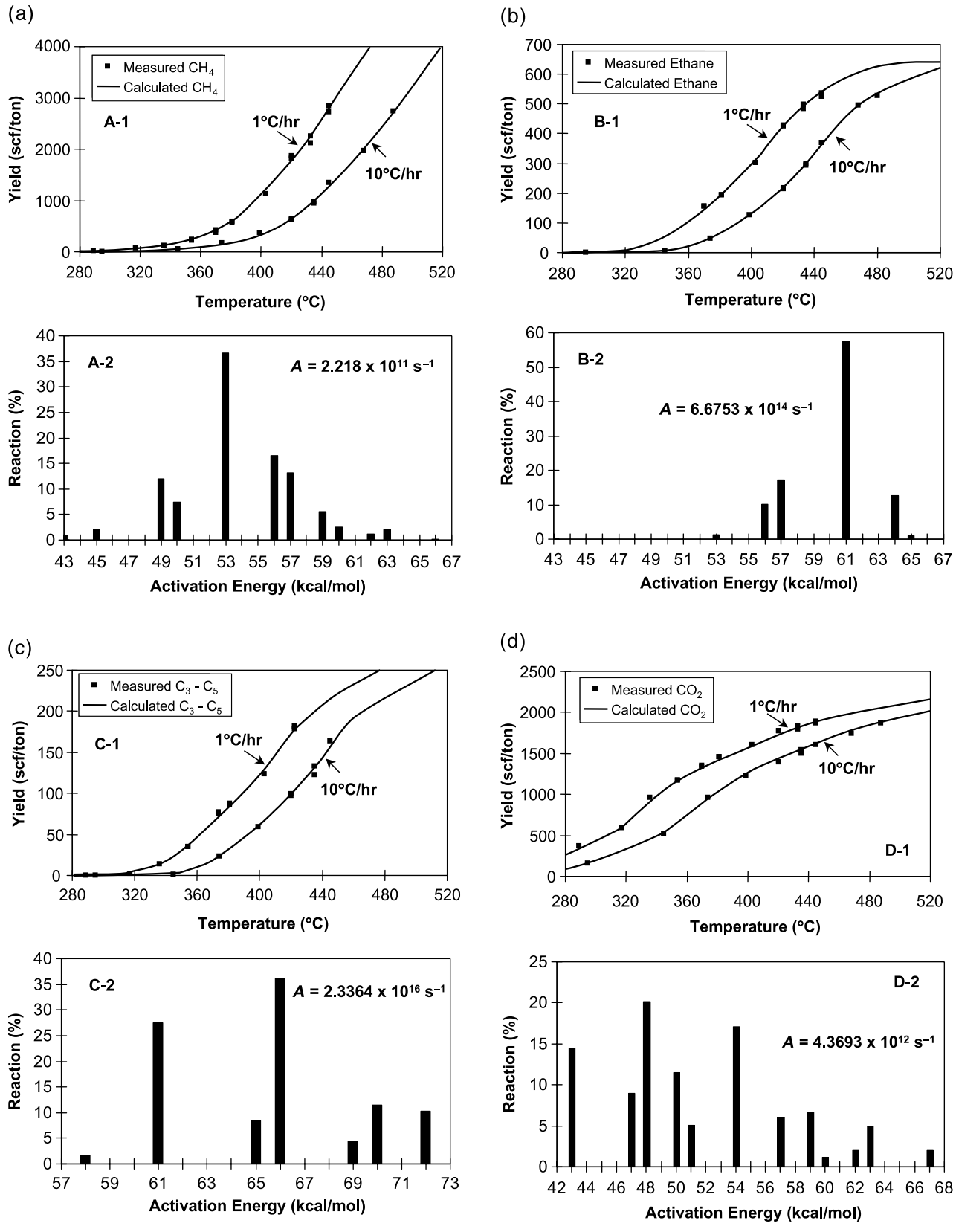

Figure 5. Best curve fittings and the kinetic parameter sets for the generation of methane (A-1 and A-2), ethane (B-1 and B-2), C_3–C_5 hydrocarbons (C-1 and C-2), and CO_2 (D-1 and D-2) from the Cameo coal in the Twin Arrow 4-14 C&K well. A = frequency factor in 1/s.

Table 4. Kinetic Parameters for Vitrinite Reflectance, C_1-C_5, and CO_2 (scf/ton, dry-ash-free coal) for the Pyrolysis of the Cameo Coal from the Twin Arrow 4-14 C&K Well, Piceance Basin, Northwestern Colorado

Component	R_o (%)	Methane	Ethane	C_3-C_5	CO_2
Maximum Yield	3	5770	640	380	2240
A (s^{-1})*	1.3952×10^{13}	2.218×10^{11}	6.6753×10^{14}	2.3364×10^{16}	4.3693×10^{12}
E (kcal/mol)**	Reaction (%)	Reaction (%)	Reaction (%)	Reaction (%)	Reaction (%)
43	11.23	0.77			14.44
44	0	0			0
45	0	2.04			0
46	0	0			0
47	0	0			9.01
48	0.38	0			20.18
49	0	12.02			0
50	9.46	7.36			11.53
51	0	0			5.02
52	1.6	0			0
53	1.91	36.62	1.36		0
54	4.18	0	0		17.1
55	0	0	0		0
56	5.12	16.48	10.19		0
57	0.7	13.17	17.11		6.02
58	0	0	0	1.75	0
59	0	5.49	0	0	6.68
60	0	2.56	0	0	1.11
61	0	0	57.57	27.46	0
62	5.36	1.22	0	0	1.96
63	60.05	1.99	0	0	4.91
64		0	12.73	0	0
65		0	1.04	8.46	0
66		0.23		36.12	0
67		0.05		0	2.04
68				0	
69				4.43	
70				11.45	
71				0	
72				10.32	

*A = frequency factor.
**E = activation energy.

70% of the reactions below 54 kcal/mol (Figure 5d). Compared with hydrocarbon gas production, this much lower activation energy distribution for CO_2 indicates that it is produced via the early cracking of coal organic matter, possibly through decarboxylation reactions, which is consistent with the pyrolysis data that show an early significant production of CO_2 at low-temperature conditions.

Kinetics of Vitrinite Reflectance Evolution

Figure 6 shows the best fit of the calculated R_o data from our kinetic model with those observed from the pyrolysis experiments. The values of the frequency factor and activation energies are listed in Table 4 and graphically presented in Figure 6. The results indicate that the R_o evolution of the

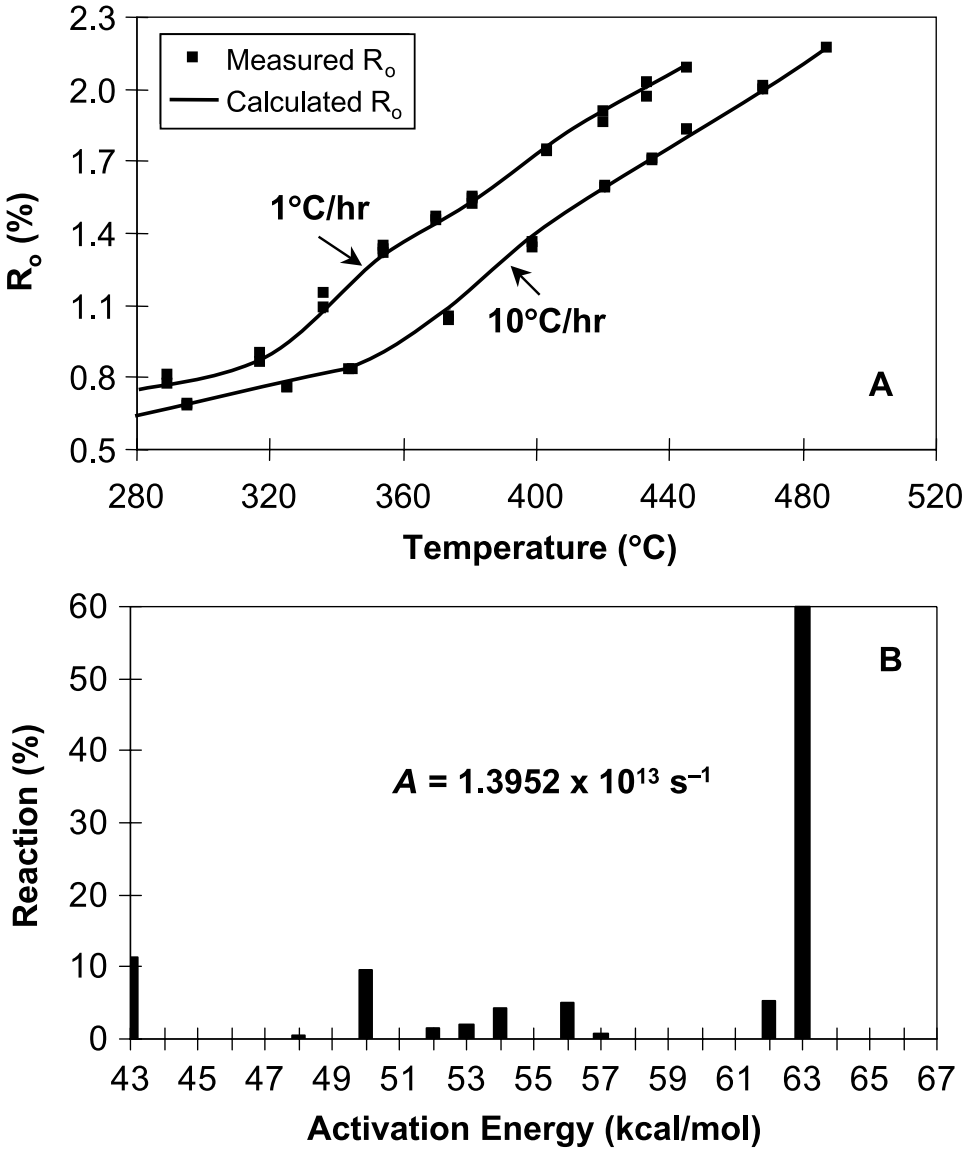

Figure 6. Best curve fitting (A) and the kinetic parameter set (B) for the R_o evolution from the Cameo coal in the Twin Arrow 4-14 C&K well. A = frequency factor in 1/s.

Cameo coal can be described best with a frequency factor of $1.3952 \times 10^{13}\ s^{-1}$ and activation energies ranging between 43 and 63 kcal/mol. To understand our model's prediction, a comparison of calculated data with observed data for the Cameo coal was made using pre-existing R_o and our R_o kinetic models. The results show that our model gives a better match between predicted and measured R_o values. This indicates that the kinetic behavior of organic maturation can be significantly different for different coals and kerogens because of compositional variability. Because our kinetic model was calibrated by pyrolysis data that have the R_o range from 0.5 to 2.2%, it may be used with confidence from 0.6 to 2.1%. This reflectance range is large enough to cover the coal-rank sequence in the Piceance Basin.

Basin Modeling

Using the basin-modeling procedures described previously, constrained by a thorough understanding of the burial history and thermal history of the Cameo coal, we mapped not only the regional coal-rank patterns but also the basinwide gas kitchen of the coal. To describe the resulting models clearly, we review first the results of our reconstruction of the burial and thermal histories of the Cameo coal.

Table 5. Prediction of Coal Maturity, Gas Content, and Total Volume of Methane Generated from the Cameo Coal for Wells in the Piceance Basin, Northwestern Colorado, from 1-D Basin Models

Well No.	Operator	Lease	Well Name	Township	Range	Section	R_o(%)	R_o Lit.*	CH_4**	CO_2**	Wetness†	Coal (ft)††	F_{vc}‡	CH_4 (bcf/mi^2)
1	Buckhorn Oil	California Federal	N	N009	W087	24	0.62		34	232	0.02	5	0.938	0.17
4	Forest	Krause	15-1	N004	W097	15	0.62	0.65[a]	38	240	0.03	35	0.938	1.32
5	Cities Service Oil	Federal Preece	B-1	N003	W096	19	0.72	0.62[a]	95	301	0.21	57	0.938	5.43
7	Fuel Resources Dev. Co.	Federal	1	N002	W096	31	0.80	0.67[a]	82	293	0.15	45	0.938	3.68
8	Cities Service Oil	Federal	4A	N002	W097	26	0.69	0.67[a]	65	272	0.10	19	0.938	1.25
11			CR-2	N001	W097	36	1.59		1277	526	1.43	39	0.936	51.60
12	Pacific Trans Supp	Barcus Creek	22-12	N001	W099	12	0.95		168	382	0.45	20	0.938	3.37
13	Jack Grynburg	Govt.	1	N001	W100	5	0.86	0.60[a]	123	321	0.30	20	0.938	2.45
14	Chorney	East Rangely Govt.	1-14	N001	W100	14	0.80	0.65[a]	82	295	0.16	20	0.938	1.64
16	USGS		CH-4	S001	W095	9	1.33[a]		469	480	1.50	72	0.937	34.20
17	USGS		C-299	S001	W097	29	1.46[a]		952	518	1.51	45	0.937	43.87
18	USGS	Colorado Min.	14-1	S001	W098	14	1.38[a]		697	506	1.51	29	0.937	20.57
19	Colorado Minerals		28-1	S001	W098	28	1.50		1081	521	1.49	40	0.936	44.42
20	Munson	Chevron	36-1-100	S001	W100	36	0.66	0.73[a]	55	263	0.05	15	0.938	0.83
21	Twin Arrows	N. Douglas Creek	4-31	S001	W101	31	0.40		0	0	0.00	5	0.939	0.00
22	?			S002	W095	14	1.42		796	509	1.52	50	0.937	40.62
23	?			S002	W095	26	1.36		642	497	1.41	50	0.937	32.62
24	Mobil Oil	Mobil	T-52-19G	S002	W096	19	1.93	1.56[a]	2516	586	1.68	50	0.934	134.77
25	Mobil Oil		T67-13G	S002	W097	13	1.52		1147	523	1.42	45	0.936	53.14
26	Mobil Oil	PCU	31-13	S002	W097	13	1.61		1309	535	1.42	45	0.936	61.20
27	Pan Am	Peterson	1	S002	W098	4	1.40		767	508	1.47	42	0.937	32.84
28	Rio Blanco	Govt.	298-29-2	S002	W098	29	1.67	1.26[a]	1442	540	1.41	45	0.935	67.79
29	?			S003	W094	35	0.48		0	0	0.00	5	0.938	0.00
30	?			S003	W095	24	1.82		1976	567	1.51	50	0.934	104.72
31	C.E. Chancellor	Govt. Hunter Creek	397-3-1	S003	W097	3	1.64	1.80[a]	1365	538	1.41	48	0.935	68.22
32	CSG Expl.	Govt.	398-33	S003	W098	33	1.38	1.35[a]	724	508	1.49	48	0.937	35.39
33	Twin Arrow	C&K	4-14	S003	W101	14	0.50	0.50[a]	0	0	0.00	5	0.939	0.00
34	Fuelco Texas Mt.	Federal	8-1	S003	W102	8	0.46	0.52[a]	0	0	0.00	5	0.938	0.00
35	Fuel Resources Dev. Co.	Texas Mtn.	16-2	S003	W102	16	0.36	0.51[a]	0	0	0.00	5	0.939	0.00
36	Fuelco Texas Mt.	Federal	21-2	S003	W102	21	0.38		0	0	0.00	5	0.939	0.00
37	ARCO	North Rifle	1	S004	W093	31	0.88		130	345	0.34	45	0.938	5.87
38	?			S004	W094	3	1.45		922	516	1.44	55	0.937	51.89
40	Chevron		1-25	S005	W099	25	1.36		601	497	1.51	15	0.937	9.16
41	Tipperary	Sky. Hydro.	2	S005	W100	13	0.63		42	249	0.03	10	0.938	0.42

42	Tipperary	Bear Gulch	1-30F	S005	W100	30	0.63	0.63[a]	43	253	0.03	10	0.938	0.43
43	Snyder Oil Co.	Barton Porter	1-16	S006	W090	16	1.02	1.04[a]	184	412	0.53	50	0.938	9.20
44	Snyder Oil	Jolley	1-8	S006	W091	8	1.51	1.45[a]	1111	524	1.48	65	0.936	74.30
45	Koch Exploration	Frick MC	11-26	S006	W092	26	1.57		1217	529	1.43	65	0.936	81.83
46	ARCO-Exxon		1-36	S006	W093	36	1.67	1.60[a]	1441	545	1.43	70	0.935	105.37
47	CER Corp.	MWX	1&2	S006	W094	34	1.79	1.90[b]	1975	560	1.49	90	0.935	187.82
48	Barrett Energy Co.	Crystal Creek Fee	A-2	S006	W097	23	1.53	1.70[b]	1141	526	1.45	60	0.936	70.54
49	Chevron	Skinner Ridge	4-2	S006	W098	28	0.83		103	314	0.25	32	0.938	3.29
50	TRW Exploration	Sunlight Federal	2	S007	W089	32	0.85		115	332	0.28	50	0.938	5.76
51	Dome	Baldy Creek Unit	1	S007	W090	17	1.61	2.10[a]	1337	535	1.39	50	0.936	69.45
52	Tenneco REI	Cameo Fee	20-4	S007	W091	20	1.25	1.50[a]	298	457	1.06	64	0.938	19.22
53	Mobil Oil	Connell	1	S007	W092	34	1.06	1.70[a]	196	440	0.59	70	0.938	13.75
55	El Paso Natural Gas	Standard Shale	1	S007	W099	6	0.71	0.74[a]	61	267	0.07	38	0.938	2.33
56	Chevron	Divide Creek	1	S008	W091	36	0.79	0.80[a]	77	292	0.13	50	0.938	3.84
57	Resources Ent. Inc.	Deep Seam 32-2	1	S009	W094	32	1.09		204	423	0.63	65	0.938	13.24
58	Teton	Sparks	36-4	S009	W095	36	1.29		389	470	1.24	60	0.937	23.62
59	Exxon	D. K. Estate	?	S009	W095	11	1.33	1.35[a]	481	480	1.45	62	0.937	30.24
60	Ralston Production Co.	Federal	31	S010	W090	31	0.86	0.90[a]	123	342	0.32	60	0.938	7.40
61	Chevron	Oxy. Cascade Creek	604-1	S006	W097	4	1.34		499	486	1.77	45	0.937	22.79
62	Chevron	Skinner Ridge	65-12D	S005	W097	12	1.24		291	456	0.99	45	0.938	13.21
63	Chevron	Trail Ridge	1-23	S005	W097	23	1.25		304	457	1.09	38	0.938	11.66
64	Exxon	Old Man Mtn.	2	S010	W095	36	0.69	0.70[a]	61	268	0.08	33	0.938	2.02
65	Chevron USA Inc.	Trail Ridge	5-19	S005	W096	19	1.70		1426	543	1.43	42	0.935	62.76

*R_o Lit. = R_o values cited from literature: [a]Nuccio and Johnson (1983); [b]Johnson and Nuccio (1993).

**Gas content: scf/ton, reserved dry-ash-free coal.

†Gas wetness: $[\sum(C_2 - C_5)/\sum(C_1 - C_5) \times 100]$.

††Net coal thickness of the Cameo seams determined from borehole data.

‡F_{vc} = correction factor that relates the weight percent ash-free coal (F_{wc}) and ash yield (F_{wa}) determined from proximate data to the coal-volume fraction (Scott et al., 1995): $F_{vc} = (F_{wc} \times \rho_a)/(F_{wc} \times \rho_a + F_{wa} \times \rho_c)$, where ρ_a is the density of ash-forming minerals ($\sim$2.65 g/cm^3) and ρ_c is the density of ash-free coal.

Burial History of the Cameo Coal

During the Late Cretaceous (93–65 Ma), the Piceance Basin was located along the western margin of the Western Interior seaway and received the sediment that composed the Mancos Shale (base) through the Iles and Williams Fork formations (Figure 1). The Cameo coal zone is composed predominantly of carbonaceous shale, coal, and sandstone. These strata grade upward into the sandier and less coaly upper part of the Williams Fork Formation. The formation generally thickens eastward from about 1500 ft (460 m) in the Douglas Creek arch on the west to reach a maximum thickness of about 4500 ft (1370 m) along the eastern structural trough of the basin (Figure 1). A basinwide unconformity is at the top of the Williams Fork (Johnson and May, 1978, 1980). The thickness of Cretaceous rocks removed by erosion is unknown. However, the Cameo coal during that time was not buried deeply, and coalification temperatures were low (Johnson and Nuccio, 1986; Law et al., 1989). Therefore, that part of the burial history is depicted as a period of nondeposition instead of erosion, an assumption that should not have a significant effect on the thermal history calibration.

Following this period of nondeposition, subsidence and sedimentation resumed in the early or middle Paleocene. The Cameo coal underwent continuous burial as the Tertiary sediments accumulated, and the coals reached maximum burial depth at the end of the Laramide orogeny (near the end of the Eocene, ~36 Ma). The overlying Tertiary formations consist of a wide variety of sandstone, siltstone, nonmarine carbonate, and continental evaporate units that include fluvial, alluvial, and lacustrine deposits (Johnson and Nuccio, 1986). These formations are more than 12,000 ft (3750 m) thick along the eastern structural trough of the basin and thin to a minimum of about 1200 ft (366 m) over the Douglas Creek arch on the west. From 36 to 10 Ma, no evidence of deposition in the Piceance Basin is seen. However, shallow intrusions of intermediate composition were emplaced in the southeastern part of the basin about 34–29 Ma, and basaltic extrusions, which have been dated by Marvin et al. (1966) as 9.7 ± 0.5 Ma, covered much of the central part. Commencing about 10 Ma, the entire region was uplifted and eroded.

Based on well profiles (see Table 5) and published literature (Dunn, 1974; Tweto, 1975; Choate et al., 1984; Johnson and Nuccio, 1986; Johnson, 1989a, b; Franczyk et al., 1992; Tyler et al., 1996), five major episodes of deposition and erosion occurred during the burial history of the Williams Fork Formation in the Piceance Basin.

Figure 7a illustrates a burial model for the coal measures representing one of the borehole sections (Mobil T-52-19G Mobil, well 24, Table 5) in the study area. The dark lines represent the Cameo coal at the base of the 100-ft (30-m) section of the coal measures. A comparison of the three representative curves indicates that, during the depositional episode near the end of the Eocene (about 36 Ma), the maximum burial depth of the coal measures may have ranged from as little as 5000 ft (1524 m) in the west to 20,000 ft (6096 m) in the east along the eastern structural trough of the basin. Consequently, if the thickness of the coal-bearing Williams Fork increased eastward from 1500 ft (457 m) in the Douglas Creek arch to about 4500 ft (1372 m) along the basin axis, as calculated from borehole data, the maximum thickness of the Tertiary rocks must have ranged between 7500 ft (2286 m) in the west and 15,000 ft (4572 m) in the central part of the basin. Between 10 Ma and the present, the central Piceance Basin underwent a rapid and substantial uplift, causing rapid erosion, in response to the main phase of Laramide tectonism. However, in the western Piceance Basin, erosion appears to have occurred relatively slow.

Thermal History of the Cameo Coal

Based on average thermal conductivities and downhole temperature data, the present-day geothermal gradients and heat-flow values for each borehole were calculated. The results show that the present-day geothermal gradient ranges from 28.8°C/km in the northeastern part of the basin to 43.2°C/km in the southwestern part, which agrees with the estimates of Johnson and Nuccio (1986). Similarly, the present-day surface heat flow increases from about 50 mW/m^2 in the north to approximate 65 mW/m^2 in the south. Monroe and Sass (1974) and Reiter

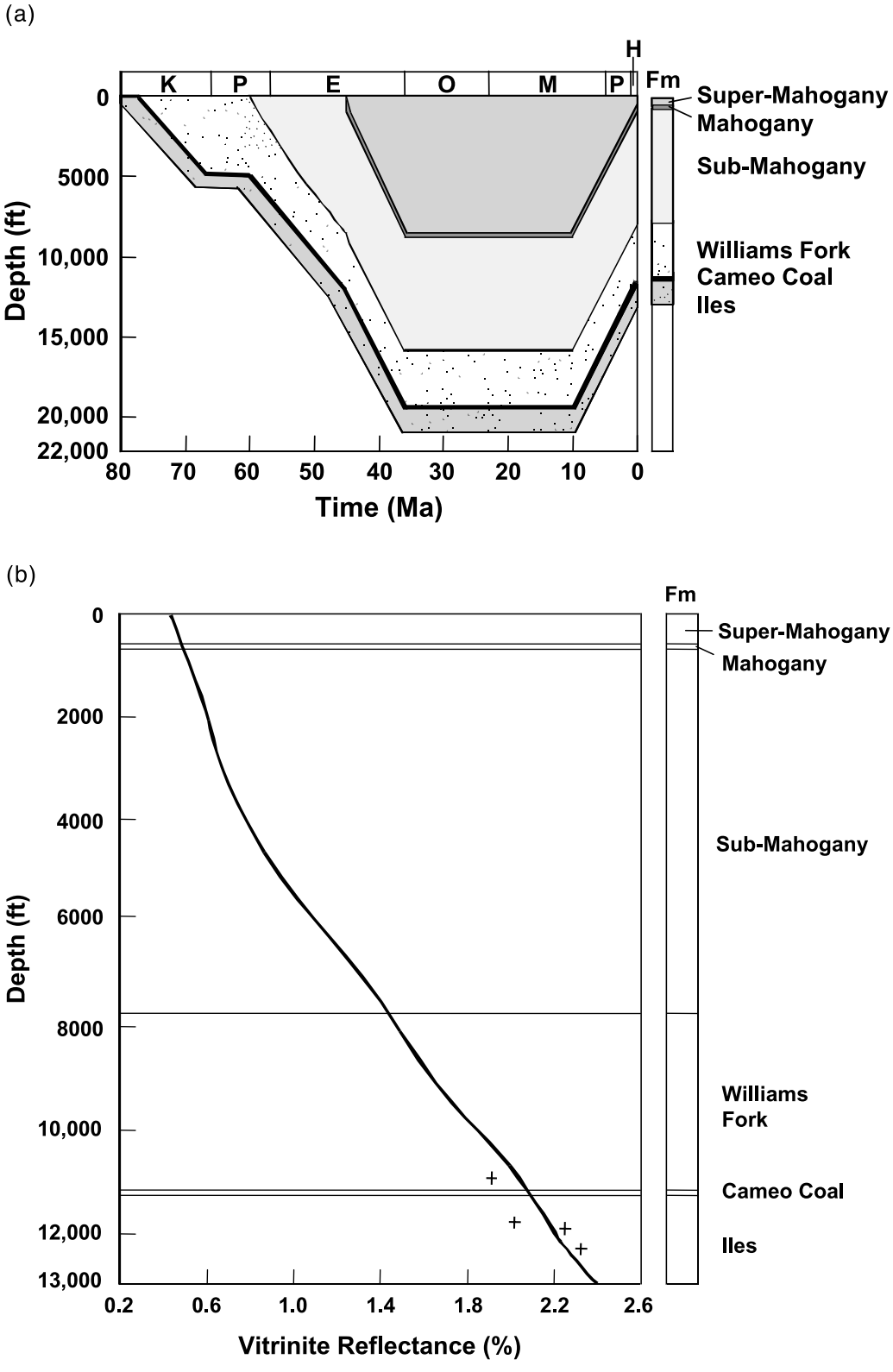

Figure 7. (a) Representative burial history curve of the Cameo coal zone in the Mobil T-52-19G Mobil well (well 24, Table 5), Piceance Basin, northwest Colorado. K = Cretaceous; P = Paleocence; E = Eocene; O = Oligocene; M = Miocene; P = Pliocene; H = Holocene. (b) Calculated R_o profile (shown as a curve) with measured R_o profile (shown as +) showing a good agreement between measured and model R_o values. Mahogany refers to the Mahogany oil-shale zone, which is an important stratigraphic marker in the upper part of the Green River Formation in the basin.

et al. (1975, 1979) also calculated the regional heat flow for the Piceance and adjacent basins. Their results showed the heat-flow values to range between 58.5 mW/m^2 (1.4 heat-flow unit [HFU]) and 83.6 mW/m^2 (2.0 HFU), which are in good agreement with those used in the present study.

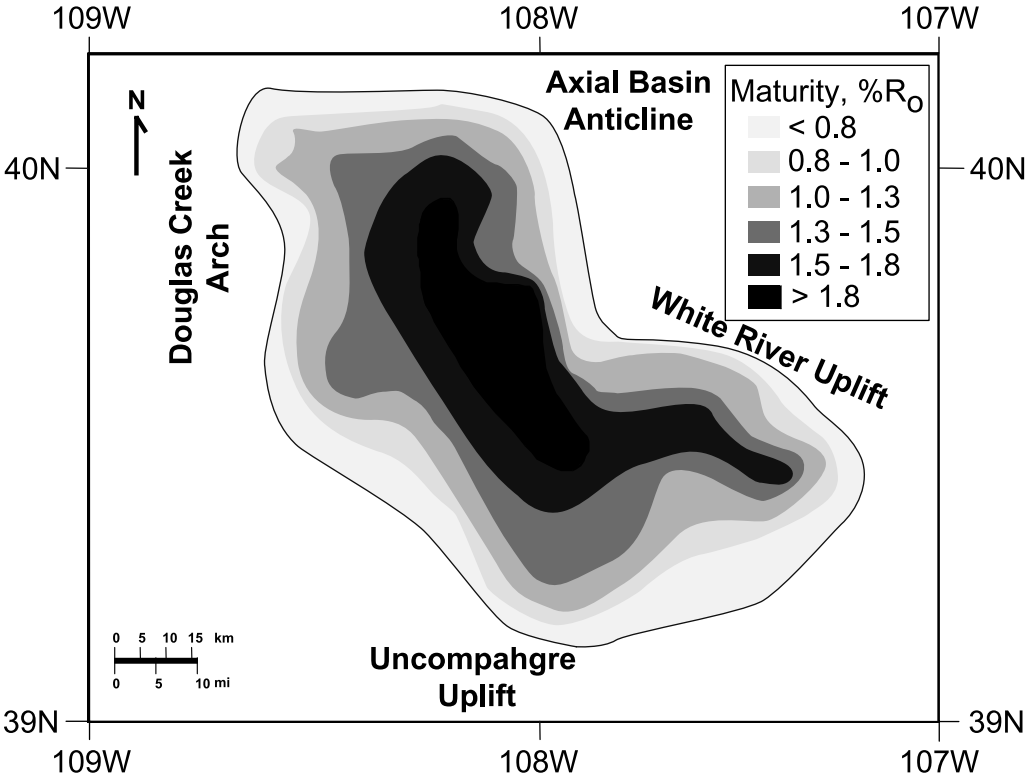

Figure 8. Isoreflectance (%R_o) contour map of the Cameo coal, Piceance Basin, northwestern Colorado.

Evidence that present-day heat flow can be applied through modeled time exists. Oligocene through Miocene magmatism occurred in the southern part of the basin, and nonsteady state thermal regimes may have dominated in localized areas of the Piceance Basin during that time. In this study, possible variations of paleoheat flow through time were investigated with two assumptions in the thermal modeling: (1) present-day heat flow persisted in the basin throughout its burial history, and (2) heat flow was in a nonsteady state during the Oligocene–Miocene, but constant since then and at the levels of present-day values.

Figure 7b shows the data-matching result for the observed R_o profile for the Mobil T-52-19G Mobil well (well 24, Table 5) versus the modeled maturity. In general, the fit of the calculated maturity profile with the measured R_o data supports the regional coal-rank patterns resulting from maximum burial and normal heat flow similar to the modern-day values. In the southern part of the basin, however, in borehole CER Corporation 1&2 MWX (well 47, Table 5), a paleoheat flow of 10 mW/m^2 higher than the present-day heat flow must be invoked to match the R_o profiles. If all other parameters used in the thermal modeling are valid, this would indicate that anomalous heating associated with Oligocene magmatic activity in the southern part of the basin has influenced the local coal-rank variation and gas generation.

DISCUSSION

Vitrinite Reflectance Kinetics

Several approaches exist for the kinetic modeling of changes in R_o with increased thermal stress. These approaches are presumed universally applicable to all kerogen or coal and therefore universally suitable for comparisons with laboratory pyrolysis data. However, in our study, we were unable to match the Cameo coal experimental results using a preexisting kinetic approach and had to develop our own basin-specific R_o kinetic model. This is not completely surprising because not all kerogens or all coals are chemically alike. Considerable natural variability in huminite or R_o at all coal ranks within

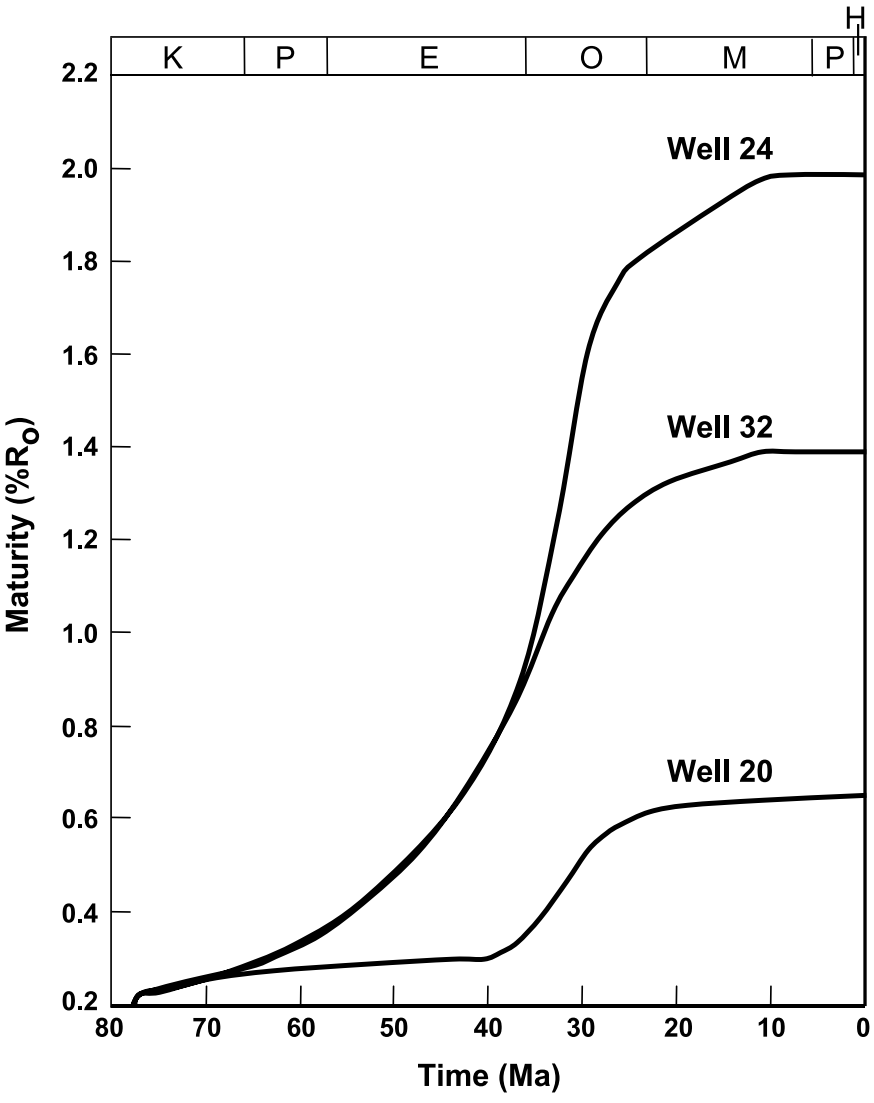

Figure 9. Maturation histories of the Cameo coal in three representative boreholes: well 20, Munson 36-1-100 (Table 5; basin west flank); well 32, CGS Exploration 398-33 (Table 5); and well 24, Mobil T-52-19G Mobil (Table 5; basin eastern center), Piceance Basin, northwestern Colorado. K = Cretaceous; P = Paleocence; E = Eocene; O = Oligocene; M = Miocene; P = Pliocene; H = Holocene.

sedimentary basins that results from factors not related to thermal history is observed, including variability in the types and amounts of original biopolymers contributing to the organic matter and the depositional environments where organic matter accumulates (Stach et al., 1982; Rathbone and Davis, 1993; Lewan, 1994). This underscores the need for the development of basin-specific R_o kinetic models in this type of study.

Coal Maturity Pattern

Figure 8 is a revised regional coal-rank map for the Piceance Basin assembled from R_o data and is similar to the map published by Johnson and Nuccio (1986). The margin of the basin is roughly defined by the 0.45–0.5% R_o contour line, whereas the center of the basin reached 1.95% R_o as observed in the well data from the Cameo coal. Johnson and Nuccio (1986) showed R_o reaching 2.1% in the Piceance Basin west of Rifle, Colorado. Based on R_o, the Cameo coal seams range in rank from subbituminous B to high-volatile C bituminous (northeast, west, and south margins) to semianthracite (eastern and central regions and along the synclinal axis). The coals adjacent to Oligocene magmatic intrusions reach anthracite rank, and graphite has been reported locally (Collins, 1976).

Our own analysis of the R_o data, summarized in the isoreflectance contour lines (Figure 8), shows

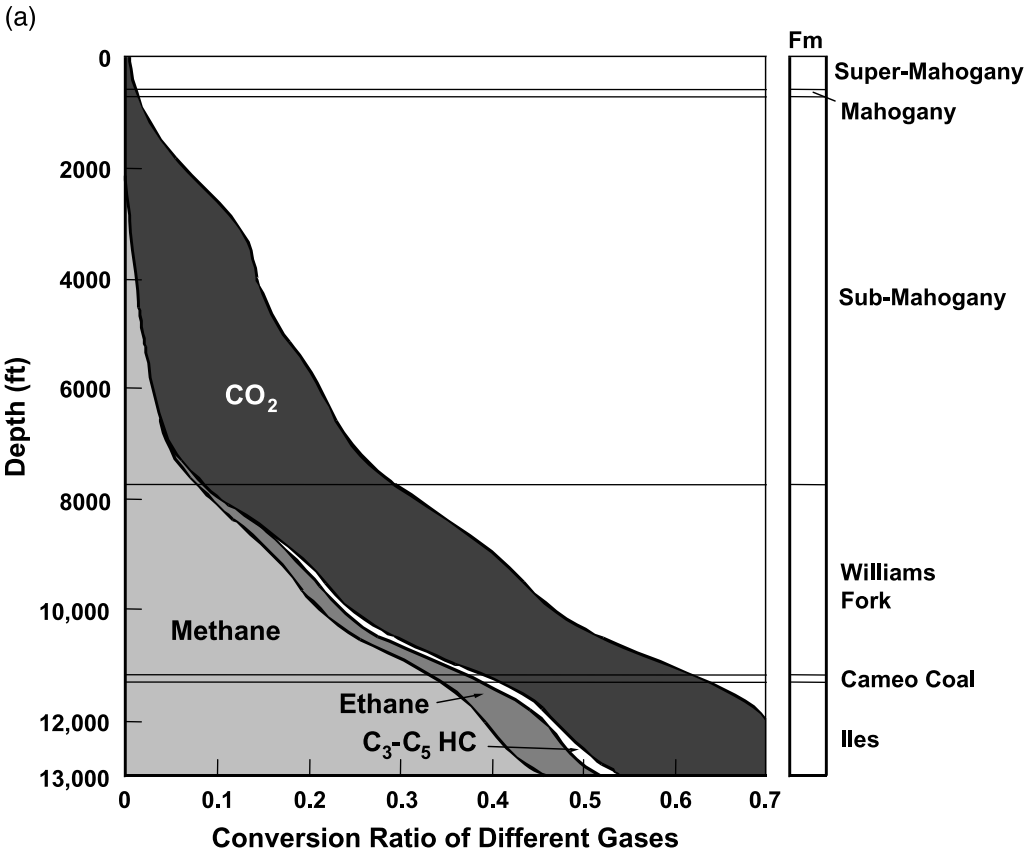

Figure 10. (a) Modeled gas generation from the Mobil T-52-19G Mobil well (well 24, Table 5) using gas generation kinetic parameters derived in this study. (b) Methane generation histories of the Cameo coal in three representative boreholes: well 20, Munson 36-1-100 (Table 5; basin west flank); well 32, CGS Exploration 398-33 (Table 5); and well 24, Mobil T-52-19G Mobil (Table 5; basin eastern center), Piceance Basin, northwestern Colorado. K = Cretaceous; P = Paleocence; E = Eocene; O = Oligocene; M = Miocene; P = Pliocene; H = Holocene.

that coal rank increases gradually eastward from the west and southwest basin flanks. Coal rank increases rapidly westward from the Grand Hogback (west side of the White River uplift, Figure 1) into low-volatile bituminous and semianthracite along the eastern axis of the basin. This maturity trend generally follows the regional structural configuration on the base of the Williams Fork Formation (cross section AA′, Figure 1), suggesting that most of the thermal maturation of the Cameo coal preceded or occurred concurrently with regional structural movement (Johnson and Nuccio, 1986). The timing of the Cameo coal maturation can be further assessed through basin modeling using the kinetics of this study. Figure 9 illustrates the maturation history of the coal measures predicted by the basin modeling of three borehole sections representing the western, transitional, and central parts of the Piceance Basin (Figure 1; well 20, Munson 36-1-100, Table 5; well 32, CSG Exploration 398-33, Table 5; well 24, Mobil T-52-19G Mobil, Table 5). A comparison of the borehole data (Figure 9) indicates that the coal measures on the west side of the basin (well 20) probably reached present-day coalification levels during the late Oligocene (ca. 25 Ma). In the central part of the basin (wells 32 and 24), however, coalification continued to 10 Ma when significant uplift and subsequent erosion occurred.

In addition, the systematic increase in the thermal maturity of the coals is generally correlated to overburden thickness changes as estimated from basinwide modeling. This indicates that the regional geothermal heating caused by burial was probably the dominant heat source responsible for the coal maturation, except in the southeastern corner of the basin where magmatic activity from 35 to 10 Ma raised the local geothermal gradient resulting in the anthracite rank of coal in a limited area (Collins, 1976; Johnson and Nuccio, 1986). Although late-stage hydrologic recharge along the basin margins might have introduced short-term temperature effects, these appear to have been relatively minor in terms of the overall effective heating

(b)

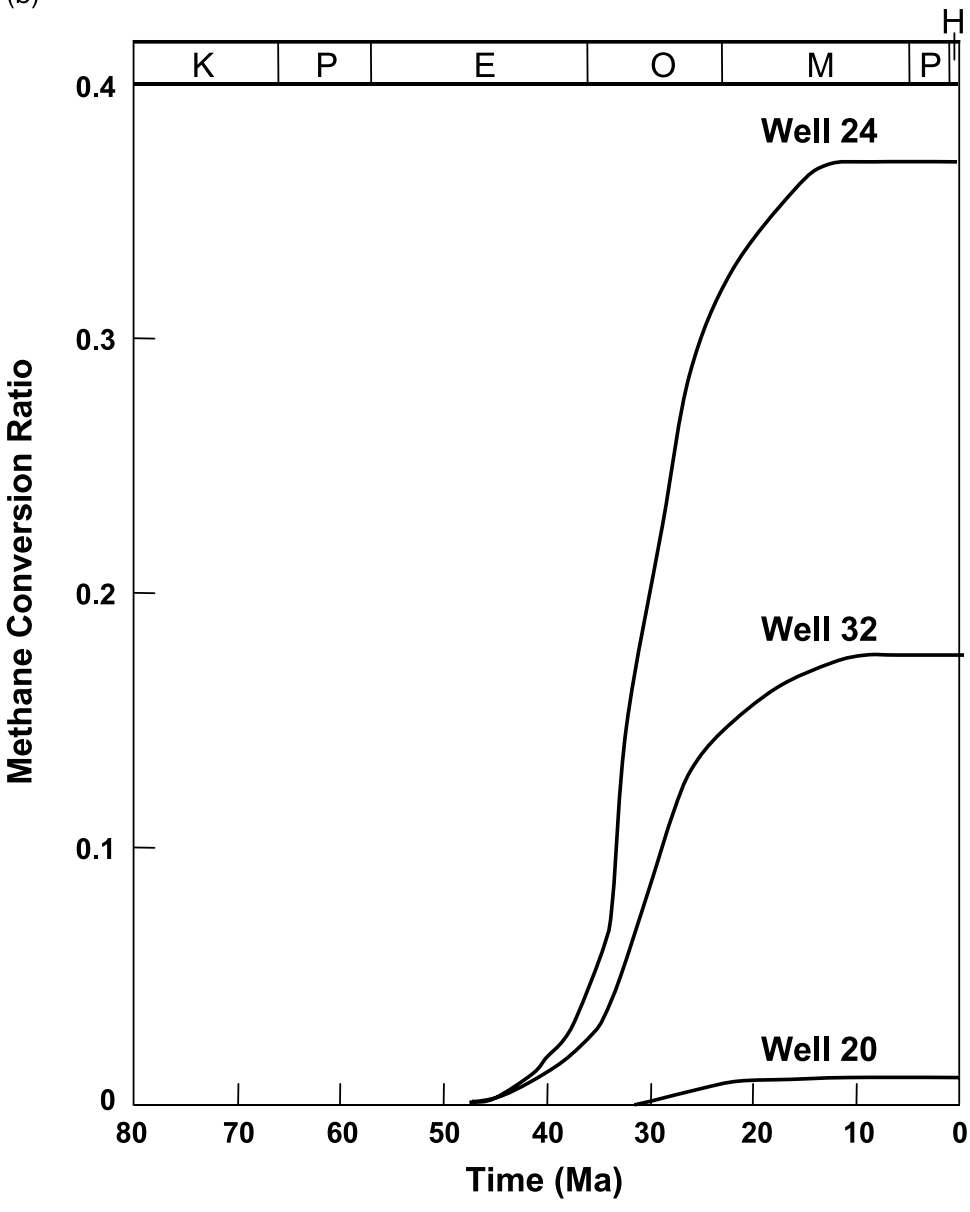

Figure 10. Continued.

time and probably had a minor influence on the overall thermal and maturation history of the Cameo coal.

Gas Generation from Cameo Coals

As mentioned previously, the modeling of gas generation from the Cameo coal was accomplished using kinetic parameters derived from the pyrolysis for methane, C_2, C_3–C_5 hydrocarbon gases, and CO_2. The thermal history of the Cameo coal was approximated using R_o kinetics from pyrolysis and by adjusting the heat flow in basin modeling to fit the observed R_o profiles from various well sites. The results of modeling gas generation versus present-day depth and geological time are presented in Figure 10a and b for three representative well locations. In the central part of the basin represented by the Mobil T-52-19G Mobil well (well 24, Table 5), the main phase of gas generation started at 45 Ma and continued until 10 Ma when temperatures dropped because of uplift and erosion. At this location, the modeling of gas generation from the Cameo coal resulted in 2516 scf/ton

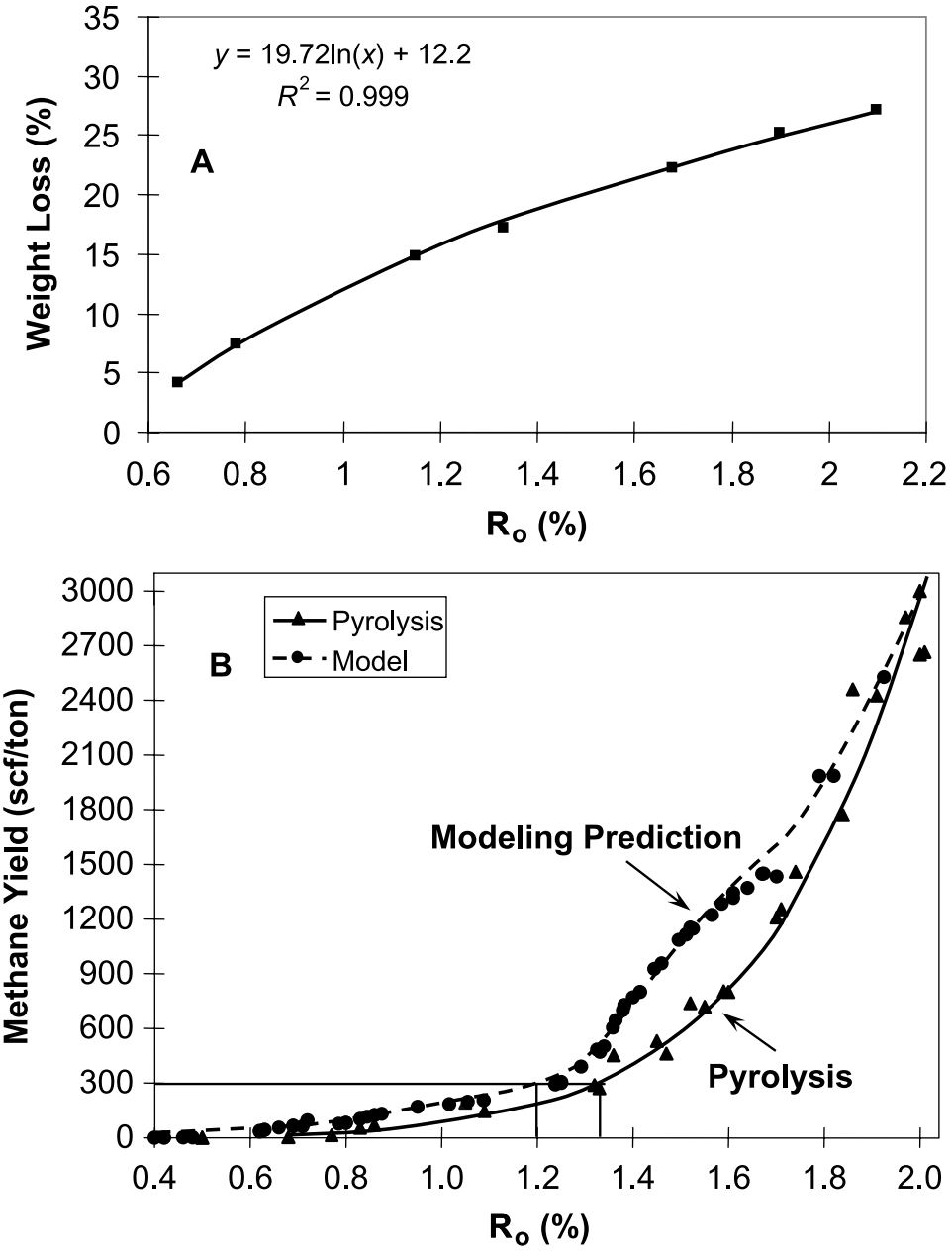

Figure 11. (A) Percent weight loss during maturation of the Cameo coal from 0.5 to 2.2% R_o. y = equation for the best-fit curve, ln(x) is natural logarithm of x while x = % R_o in a range from 0.5 to 2.2% R_o, R^2 = sum of squares residual. (B) Comparison of methane generation vs. coal rank (%R_o) from the prediction of basin modeling (in solid circle and dash curve) in this study and from the pyrolysis experiments (in solid triangle and curve) for the in-situ dry-ash-free Cameo coal, Piceance Basin, northwestern Colorado.

methane, 32 scf/ton C_2-C_5 hydrocarbon gases, and 439 scf/ton CO_2 of initial dry-ash-free Cameo coal.

In contrast, along the west flank of the basin in a section represented by the Munson 36-1-100 well (well 20, Table 5), coals were not buried deep enough to result in significant thermogenic hydrocarbon generation. Therefore, aside from possible late-stage bacterial methanogenesis associated with potential recharge paths along the basin margins (Tyler et al., 1996), mainly CO_2 generation is predicted at that location, commencing at about 30 Ma and reaching its highest level at 20 Ma, then decreasing to very little (if any) because temperatures became too low. The total yield of CO_2 is 253 scf/ton of initial dry-ash-free coal, accounting for about 83% of the total gases generated from the Cameo coal. Yields of methane and C_2–C_5 hydrocarbon gases are only 53 scf/ton dry-ash-free coal. Thus, in reservoirs on the basin's flank, one would not expect gas charge from the underlying Cameo seams, except possibly gas of biogenic origin.

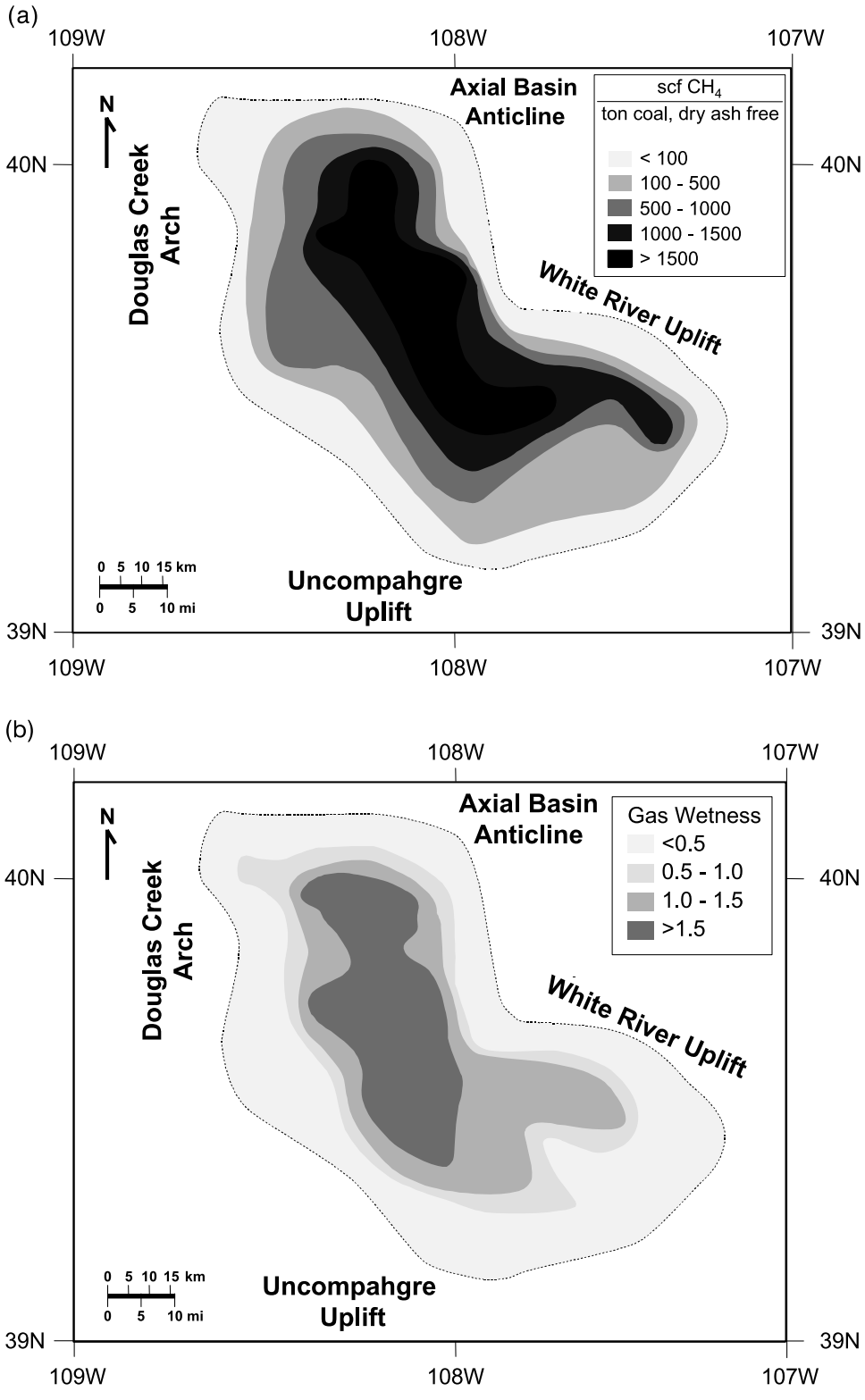

Figure 12. (a) Methane generation potentials (scf/ton, dry-ash-free coal) for in-situ Cameo coal and (b) gas wetness [$\sum(C_2 - C_5)/\sum(C_1 - C_5) \times 100$] for the gases generated from the Cameo coal, Piceance Basin, northwestern Colorado, predicted from basin modeling using the gas generation kinetics derived in this study.

To calculate gas yields relative to the weight of in-situ coal, coal weight loss because of the generation of water and gases during coalification must be considered. Our pyrolysis data show approximately 25% weight loss (based on the mass of original starting coal) during coalification from subbituminous A or high-volatile C bituminous at 0.5% R_o to semianthracite rank on the dry-ash-free basis

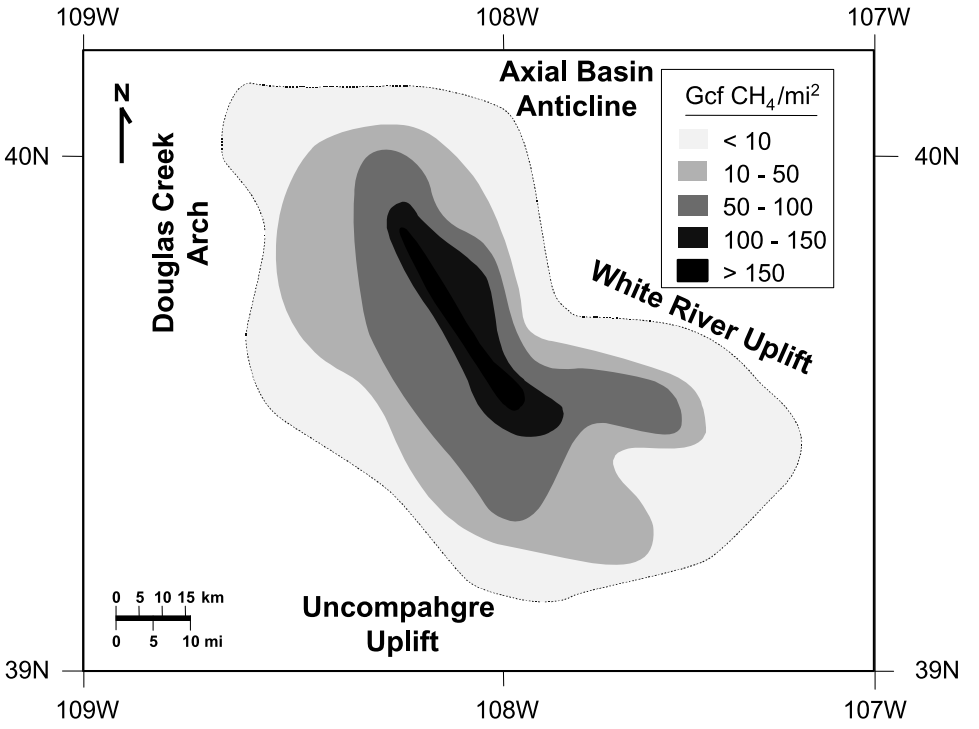

Figure 13. Total volume of methane generated from the Cameo coal, Piceance Basin, northwestern Colorado, predicted from basin modeling using the gas generation kinetics derived in this study. The contour map is constructed using the total net coal thickness map and Piceance Basin modeling results, including coal-rank (%R_o) and gas yield data. The contour interval is 10 bcf/mi^2.

(Figure 11A). The total gas yields from modeling in the central part of the basin as represented by the Mobil T-52-19G Mobil well (well 24, Table 5) are estimated to be approximately 2516 scf/ton methane, 43 scf/ton C_2–C_5 hydrocarbon gases, and 586 scf/ton CO_2 of in-situ dry-ash-free Cameo coal. Compared with the pyrolysis data shown in Figure 11B, the methane yield is slightly higher at geological conditions than the value of 2427 scf/ton methane of in-situ dry-ash-free coal measured from pyrolysis experiments of the Cameo coal. Furthermore, the model probably underpredicts gas values in the southwestern part of the basin. The detailed gas prediction results are reported in Table 5.

Variations in total methane yield and gas wetness across the Piceance Basin are shown in Figure 12a and b. The predicted methane yield increases from less than 100 scf/ton of in-situ coal from basin flanks where R_o values are between 0.5 and 0.7% to more than 2500 scf/ton in the deep northern and southeastern troughs of the basin where coal rank reached the semianthracite level (1.93%). The generation of significant quantities of methane (e.g., $\geq$300 scf/ton) started at 1.2% R_o and exceeded 2500 scf/ton (in-situ dry-ash-free coal) at a coal rank of 1.93% R_o. Gases generated in both low and high maturity coals are less wet (<20% wetness), whereas wetter gases are in the area with coal ranks at 1.4–1.5% R_o (>35% wetness). Gas yields are probably underpredicted in the southern basin where R_o is underpredicted by the kinetic model (see Figure 12a, b; Table 5), but overall, the R_o model and field results show good agreement.

The CO_2 generation from the Cameo coals is also estimated as shown in Figure 10a. Modeling indicates that large quantities of CO_2 were probably generated during early coalification (R_o < 1%). However, amounts of produced CO_2 from wells are much lower than amounts predicted by modeling. One explanation is the high solubility of CO_2 in water. A. B. Carpenter and L. M. Cathles (1996, personal communication) suggested that CO_2 could be removed from gas as it migrates within a basin and reacts with silicates of calcium, magnesium, and/or iron. This theoretical prediction has been reported to be consistent with some field data, which shows that gas generated from, or migrated through, formations with initially significant Ca-Mg-Fe silicate content will generally contain less CO_2 than gas produced from rocks containing small amounts of these silicates.

Volumes of Generated Coalbed Methane

To calculate the volume of gas generated per square mile from the in-situ Cameo coal, several parameters had to be considered. These include gas content of the in-situ coal, net coal thickness, ash content, and coal density. As discussed above, the gas content has been predicted from basin modeling and corrected to an ash-free basis to remove gas content variability caused by changes in mineral matter content among coal seams. The cumulative thickness of the coal seams in the upper part of the Williams Fork Formation is based on borehole data (Table 5), and the net Cameo coal isopach map was generated from these data.

Ash content, however, is one of the difficult parameters to evaluate in calculating coalbed gas resources. Because (1) the ash content of the Cameo coals is variable, ranging from less than 1 to 47.9% across the Piceance Basin (Tremain and Toomey, 1983; McFall et al., 1986; Diamond et al., 1986), and (2) ash-content data were not available for coal seams in each borehole, an average value of 12.5% ash content as given by Tyler et al. (1996) was used for calculating ash-free gas resources.

Furthermore, the determination of ash-free coal density is more complicated. Because the density difference between ash-forming minerals (commonly greater than 2.65 g/cm^3) and ash-free coal (about 1.3 g/cm^3 for high-volatile bituminous) is so large, the weight-percent ash in coal is much greater than the actual volume-percent ash. Therefore, a correction factor that relates the weight percent of ash in coal to its volume percent needs to be considered. Accordingly, we adapted the approach established by Scott et al. (1995) to calculate the correction factor and to estimate the ash-free coal density in this study. According to Scott et al. (1995), the GIP is a function of coal volume, coal density (on dry-ash-free basis), and ash-free gas content. Thus,

$$\mathrm{GIP} = (h \times A \times F_{\mathrm{vc}}) \times \rho_{\mathrm{c}} \times \mathrm{GC} \qquad (4)$$

where GIP is the gas in place (scf), h is the coal thickness (ft), A is the area (mi^2), F_{vc} is the volume correction factor, ρ_{c} is the ash-free coal density (ton/ft mi^2), and GC is the ash-free gas content (scf/ton). The volume of the coal gas generated from the Cameo coal is reported in Table 5 and mapped in Figure 13. The results show that the area with the most in-place coalbed gas generated is located near the trough of the basin, where generation exceeds 150 bcf/mi^2. Toward the basin margins, in-place coalbed gas resources become less than 10 bcf/mi^2. The regional distribution of the coalbed gas resources generally follows R_o trends and net coal thickness variation patterns. Our kinetic study and basin-modeling predictions indicate that the Piceance Basin has great potential to contain important commercial accumulations of coalbed methane (Figure 13). In addition, measurements of coal adsorption capacity by Eddy et al. (1982) and Tyler et al. (1996) indicate that approximately 480–1000 scf of methane/ton of coal can be stored in the coals of the Cameo seams at the rank range from about 1.3 to 1.9% R_o. Because the modeling predicts that considerably more gas may be generated by the Cameo coals than the coals can store in the deeper areas of the basin, we expect that a considerable amount of methane probably migrated from the Cameo coal to nearby noncoal reservoirs.

SUMMARY AND CONCLUSIONS

Results from the confined pyrolysis of an immature, petrographically representative Cameo coal sample from the Piceance Basin show that the simulated maturation of the coal follows a Van Krevelen type III kerogen or humic coal evolution pathway. The positive relation between increasing R_o and decreasing atomic H/C and O/C ratios indicates that the sealed gold tube pyrolysis method reasonably simulates natural coal maturation. Basin-specific R_o and gas generation kinetic parameters derived from an immature Cameo coal sample are required to adequately model gas potential.

The major gas products from Cameo coal pyrolysis are methane, C_2–C_5 hydrocarbons, and CO_2. Most of the gas generated during early maturation ($R_o < 0.8\%$) is CO_2, whereas at high coal conversion ($R_o > 0.8\%$), hydrocarbon gases are dominant. The hydrocarbon gases generated from the humic

Cameo coals are less wet, having generally less than 30% C_{2+} hydrocarbon components.

Based on the specifically developed kinetic models and using the 1-D basin-modeling program, the thermal maturity modeling of 57 wells allowed the mapping of the regional coal-rank pattern and the basinwide gas kitchen. The modeling results indicate that the coal measures to the west flank of the Piceance Basin probably reached present-day coalification levels during the late Oligocene (25 Ma). In the central part of the basin, however, coalification continued until 10 Ma when significant uplift and subsequent erosion occurred. Coal rank increases gradually eastward from high-volatile C bituminous on the west and southwest basin flanks into low-volatile bituminous and semianthracite along the eastern trough, then decreases abruptly toward the sharply upturned east margin. This maturity trend generally follows the regional structural configuration on the base of the Mesaverde Group and is generally correlated to the thicknesses of the original overburden. This indicates that the regional geothermal heating caused by the depositional burial was probably the dominant heat source responsible for the regional coal-rank pattern that was established.

The modeling of gas generation showed that, in the central part of the Piceance Basin, the main phase of gas generation started at 45 Ma and continued until 10 Ma when the temperatures decreased because of uplift and subsequent erosion. Along the western and southern flanks of the basin, coal seams were shallowly buried and temperatures were never high enough to initiate a significant generation of gases other than CO_2, except possibly for biogenic gas. In this region, the major gas generation commenced at about 30 Ma and reached the highest level at 20 Ma. There was no significant generation of gas between 20 and 10 Ma.

Predicted methane yield increases from less than 10 scf/ton in-situ coal from basin flanks where R_o is between 0.5 and 0.7% to more than 2500 scf/ton coal in the deep center along the northern and southeastern segments of the basin, where coal rank reached the semianthracite level (1.93%). The generation of significant quantities of methane (e.g., $\geq$300 scf/ton) started at 1.2% R_o and exceeded 2500 scf/ton (in-situ dry-ash-free coal) at a coal rank of 1.93% R_o. Gases generated in both low- and high-maturity coals are less wet but wetter in areas with coal ranks at 1.4–1.5% R_o. The largest in-place coalbed gas resources are along the basin axis, where they are estimated to exceed 150 bcf/mi^2. Near the basin margins, in-place coalbed gas resources can range from 0 to 10 bcf/mi^2. As controlled by regional coal maturity and total net coal thickness, the regional distribution of the coalbed gas resources generally follows R_o trends and net coal thickness patterns. Overall, our study results indicate that the Piceance Basin has great potential to contain important commercial accumulations of coal-generated gas in coal beds and tight gas sands.

REFERENCES CITED

Behar, F., S. Kressmann, J. L. Rudkiewicz, and M. Vandenbroucke, 1992, Experimental simulation in a confined system and kinetic modeling of kerogen and oil cracking, *in* C. B. Eckardt, J. R. Maxwell, S. R. Larter, and D. A. C. Manning, eds., Advances in organic geochemistry 1992: Organic Geochemistry, v. 19, p. 173–189.

Behar, F., M. Vandenbroucke, Y. Tang, F. Marquis, and J. Espitalie, 1997, Thermal cracking of kerogen in open and closed systems: Determination of kinetic parameters and stoichiometric coefficients for oil and gas generation: Organic Geochemistry, v. 26, p. 321–339.

Buiskool Toxopeus, J. M. A., 1983, Selection criteria for the use of vitrinite reflectance as a maturity tool, *in* J. Brooks, ed., Petroleum geochemistry and exploration of Europe: Geological Society Special Publication 12, p. 295–307.

Burnham, A. K., R. L. Braun, H. R. Gregg, and A. M. Samoun, 1987, Comparison of methods for measuring kerogen pyrolysis rates and fitting kinetic parameters: Energy and Fuels, v. 1, p. 452–458.

Burnham, A. K., R. L. Braun, and A. M. Samoun, 1988, Further comparison of methods for measuring kerogen pyrolysis rates and fitting kinetic parameters, *in* L. Mattavelli and L. Novelli, eds., Advances in organic geochemistry 1987: Organic Geochemistry, v. 13, p. 839–845.

Burnham, A. K., and J. J. Sweeney, 1989, A chemical kinetic model of vitrinite maturation and reflectance: Geochimica et Cosmochimica Acta, v. 53, p. 2469–2657.

Bustin, R. M., 1987, Organic maturity of Late Cretaceous and Tertiary coal measures, Canadian Arctic Archipelago: International Journal of Coal Geology, v. 6, p. 71–106.

Choate, R., D. Jurich, and G. J. Saulnier, 1984, Geologic overview, coal deposits, and potential for methane recovery from coal beds, Piceance Basin, Colorado, *in* C. Rightmire, T. Eddy, G. E. Kirr, and N. James, eds., Coalbed

methane resources of the United States: AAPG Studies in Geology 17, p. 223–251.
Collins, B. A., 1976, Coal deposits of the Carbondale, Grand Hogback, and Southern Danforth Hills coal fields, eastern Piceance Basin, Colorado: Quarterly of the Colorado School of Mines, v. 71, p. 1–138.
Diamond, W. P., J. C. LaScola, and D. M. Hyman, 1986, Results of direct-method determination of the gas content of U.S. coal beds: Bureau of Mines Information Circular 9067, 94 p.
Dow, W. G., 1977, Kerogen studies and geological interpretations: Journal of Geochemical Exploration, v. 7, p. 79–99.
Dunn, H. L., 1974, Geology of petroleum in the Piceance Creek Basin, northwestern Colorado, *in* D. K. Murray, ed., Guidebook to the energy resources of the Piceance Creek Basin, Colorado: Twenty-fifth Field Conference of the Rocky Mountain Association of Geologists, p. 217–224.
Eddy, G. E., C. T. Rightmire, and C. W. Byrer, 1982, Relationship of methane content of coal rank and depth: Theoretical vs. observed: Society of Petroleum Engineers/Department of Energy unconventional gas recovery symposium, Proceedings, p. 117–122.
Espitalie, J., P. Ungerer, H. Irwin, and F. Marquis, 1988, Primary cracking of kerogens, experimenting and modeling C_1, C_2–C_5, C_6–C_{15} and C_{15+} classes of hydrocarbons formed, *in* L. Mattavelli and L. Novelli, eds., Advances in organic geochemistry 1987: Organic Geochemistry, v. 13, p. 893–900.
Franczyk, K. J., T. D. Fouch, R. C. Johnson, C. M. Molenaar, and W. A. Cobban, 1992, Late Cretaceous and early Tertiary evolution of the Uinta and Piceance basins (northeastern Utah and northwestern Colorado) and associated development of hydrocarbons, *in* L. M. H. Carter, ed., U. S. Geological Survey Circular, Report C 1074, 31 p.
Greis, R. R., 1983, North–south compression of Rocky Mountain foreland structures, *in* J. D. Lowell, ed., Rocky Mountain foreland basins and uplifts: Field Conference of the Rocky Mountain Association of Geologists, p. 9–32.
Gretener, P. E., 1981, Geothermics; using temperature in hydrocarbon exploration: AAPG Continuing Education Course Note Series 17, 156 p.
Higg, M. D., 1986, Laboratory studies into the generation of natural gas from coals, *in* J. Brooks, J. C. Goff, and B. van Hoorn, eds., Habitat of Paleozoic gas in N.W. Europe: Geological Society Special Publication 23, p. 113–120.
Hill, R. J., P. D. Jenden, Y. Tang, S. Teerman, and I. R. Kaplan, 1994, The influence of pressure on the pyrolysis of coal, *in* P. K. Mukhopadhyay and W. G. Dow, eds., Reevaluation of vitrinite reflectance as a maturity parameter: Washington, DC, ACS Books, p. 161–193.
Hill, R. J., Y. C. Tang, P. D. Jenden, and I. R. Kaplan, 1996, The influence of pressure on oil pyrolysis: Energy and Fuels, v. 10, p. 873–882.
Hunt, J. M., 1979, Petroleum geochemistry and geology: San Francisco, W. H. Freeman, 617 p.
Johnson, R. C., 1989a, Geologic history and hydrocarbon potential of Late Cretaceous-age, low-permeability reservoirs, Piceance Basin, western Colorado: U.S. Geologic Survey Bulletin 1787E, 51 p.
Johnson, R. C., 1989b, Detailed cross sections correlating Upper Cretaceous and lower Tertiary rocks between the Uinta Basin of eastern Utah and western Colorado and the Piceance Basin of western Colorado: U. S. Geological Survey Miscellaneous Investigations Series, Map No. I-1974, scale 1:4,800, 2 sheets.
Johnson, R. C., and F. May, 1978, Preliminary stratigraphic studies of the upper part of the Mesaverde Group, the Wasatch Formation, and the lower part of the Green River Formation, DeBeque area, Colorado, including environments of deposition and investigations of palynomorph assemblages: U. S. Geological Survey Miscellaneous Field Studies Map MF- 1050, scale 1:1,200, 2 sheets.
Johnson, R. C. and F. May, 1980, A study of the Cretaceous–Tertiary unconformity in the Piceance Creek Basin, Colorado: The underlying Ohio Creek Formation (Upper Cretaceous) redefined as a member of the Hunter Canyon or Mesaverde Formation: U.S. Geological Survey Bulletin, Report B 1482-B, 30 p.
Johnson, R. C., and V. F. Nuccio, 1986, Structural and thermal history of the Piceance Creek Basin, western Colorado, in relation to hydrocarbon occurrence in the Mesaverde Group, *in* C. W. Spencer and R. F. Mast, eds., Geology of tight gas reservoirs: AAPG Studies in Geology 24, p. 165–205.
Johnson, R. C., and V. F. Nuccio, 1993, Surface vitrinite reflectance study of the Uinta-Piceance Basin area, western Colorado and eastern Utah— Implications for the development of Laramide basins and uplifts: U.S. Geological Survey Bulletin 1787-DD, 38 p.
Johnson, R. C., and D. D. Rice, 1990, Occurrence and geochemistry of natural gases, Piceance Basin, northwest Colorado: AAPG Bulletin, v. 74, p. 805–829.
Johnson, R. C., R. A. Crovelli, C. W. Spencer, and R. F. Mast, 1987, An assessment of gas resources in low permeability sandstones of the Upper Cretaceous Mesaverde Group, Piceance Basin, Colorado: U.S. Geological Survey Open-File Report 87-357, 165 p.
Juntgen, H., and J. Karweil, 1966a, Formation and storage of gas in bituminous coals: Part I: Erdol und Kohle, Erdgas, Petrochemie, v. 19, p. 251–258.
Juntgen, H., and J. Karweil, 1966b, Formation and storage of gas in bituminous coals: Part II: Erdol und Kohle, Erdgas, Petrochemie, v. 19, p. 339–344.
Law, B. E., V. F. Nuccio, and R. W. Stanton, 1989, Evaluation of source-rock characteristics, thermal maturation and pressure history, of the Upper Cretaceous Cameo coal zone, Deep Seam Well, Piceance Basin, Colorado: Proceedings of the 1989 International Coalbed Methane Symposium, p. 341–353.
Lerche, I., 1990, Basin analysis: Quantitative methods volume 1: San Diego, Academic Press, 589 p.
Lewan, M. D., 1994, Identifying and understanding suppressed vitrinite reflectance through hydrous pyrolysis experiments, abstracts and program, *in* B. J. Cardott, R. Woods, and C. L. Thompson-Rizar, eds., Collected papers from the tenth Annual Meeting of the Society for

Organic Petrology Norman, Oklahoma, October 1993: Oxford, Pergamon, p. 1–3.
Marvin, R. F., H. H. Menhert, and W. M. Mountjoy, 1966, Age of basalt cap on Grand Mesa: U.S. Geological Survey Professional Paper 550-A, p. 81.
McFall, K. S., D. E. Wicks, V. A. Kuuskraa, and K. B. Sedwick, 1986, A geologic assessment of natural gas from coal seams in the Piceance Basin, Colorado: Gas Research Institute topical report, GRI 87/0060, 76 p.
Monroe, R. J., and J. H. Sass, 1974, Basic heat-flow data from western United States, *in* J. H. Sass and R. J. Monroe, eds., Basic heat-flow data from western United States: U.S. Geological Survey Open File Report 74-9, p. 3.1–3.185.
Nuccio, V. F., and R. C. Johnson, 1983, Thermal maturity map of the Cameo-Fairfield or equivalent coal zone through the Piceance Creek Basin, Colorado— A preliminary report: U.S. Geological Survey Miscellaneous Field Studies Map MF-1575, scale 1:253,440, 2 sheets.
Pitman, J. K., J. C. Pashin, J. R. Hatch, and M. B. Goldhaber, 2003, Origin of minerals in joint and cleat systems of the Pottsville Formation, Black Warrior Basin, Alabama: Implications for coalbed methane generation and production: AAPG Bulletin, v. 87, p. 713–731.
Quigely, T. M., A. S. Mackenzie, and J. R. Gray, 1987, Kinetic theory of petroleum generation, *in* B. Doligez, ed., Migration of hydrocarbons in sedimentary basins: Paris, Editions Technip, p. 646–666.
Rathbone, R. F., and A. Davis, 1993, The effects of depositional environment on vitrinite fluorescence intensity: Organic Geochemistry, v. 20, p. 177–186.
Reiter, M. A., C. L. Edwards, H. Hartman, and C. Weidman, 1975, Terrestrial heat flow along the Rio Grande rift, New Mexico and southern Colorado: Geological Society of America Bulletin, v. 86, p. 811–818.
Reiter, M., A. J. Mansure, and C. Shearer, 1979, Geothermal characteristics of the Colorado Plateau: Tectonophysics, v. 61, p. 183–195.
Scott, A. R., W. R. Kaiser, and W. B. Ayers Jr., 1994, Thermogenic and secondary biogenic gases, San Juan Basin, Colorado and New Mexico— Implications for coalbed gas producibility: AAPG Bulletin, v. 78, p. 1186–1209.
Scott, A. R., N. Zhou, and D. R. Levine, 1995, A modified approach to estimating coal and coal gas resources: Example from the Sand Wash Basin, Colorado: AAPG Bulletin, v. 79, p. 1320–1336.
Stach, E., M. T. Mackowsky, M. Teichmueller, G. H. Taylor, D. Chandra, and R. Teichmueller, 1982, Stach's textbook of coal petrology, 3d revised and enlarged ed.: Stuttgart, Germany, E. Schweizerbart'sche Verlagsbuchhandlung, 535 p.
Sundararaman, P., P. H. Merz, and R. G. Mann, 1992, Determination of kerogen activation energy distribution: Energy and Fuels, v. 6, p. 793–803.
Tang, Y., P. D. Jenden, A. Nigrini, and S. C. Teerman, 1996, Modeling early methane generation in coal: Energy and Fuels, v. 10, p. 659–671.
Throndsen, T., B. Andersen, and A. Unander, 1993, Comparison of different models for vitrinite reflectance evolution using laboratory and modeling of well data, *in* A. G. Dore, J. H. Augustson, C. Hermanrud, D. J. Stewart, and O. Sylta, eds., Basin modeling: Advances and applications: Amsterdam, Elsevier, v. 3, p. 127–133.
Tissot, B. P., and D. H. Welte, 1984, Petroleum formation and occurrence, 2d ed.: Berlin, Springer, 699 p.
Tissot, B. P., R. Pelet, and P. Ungerer, 1987, Thermal history of sedimentary basins, maturation indices, and kinetics of oil and gas generation: AAPG Bulletin, v. 71, p. 1445–1466.
Tremain, C. M., and J. Toomey, 1983, Coalbed methane desorption data: Colorado Geological Survey Open-File Report 81-4, 515 p.
Tweto, O., 1975, Laramide (Late Cretaceous–early Tertiary) orogeny in the southern Rocky Mountains, *in* B. F. Curtis, ed., Cenozoic history of the southern Rocky Mountains: Geologic Society of America Memoir 144, p. 1–44.
Tyler, R., A. R. Scott, W. R. Kaiser, H. S. Nance, and R. G. McMurry, 1996, Geologic and hydrologic controls critical to coalbed methane producibility and resource assessment: Williams Fork Formation, Piceance Basin, northwest Colorado: Topical Report December 1, 1993–November 30, 1995, Gas Research Institute Report No. GRI-95/0532, 428 p.
Ungerer, P., 1990, State of the art of research in kinetic modeling of oil formation and expulsion, *in* B. Durand and F. Behar, eds., Advances in organic geochemistry 1989: Organic Geochemistry, v. 16, p. 1–25.
Van Krevelen, D. W., 1993, Coal: Typology-physics-chemistry-constitution: Amsterdam, Elsevier Science, 979 p.
Waples, D., 1981, Organic geochemistry for exploration geologists: Minneapolis, Minnesota, Burgess Publishing Co., 151 p.
Zhao, K., and I. Lerche, 1993, Thermal maturation and burial history of the multiwell experiment site, Piceance Basin, Colorado: Application of thermal indicator tomography, *in* A. G. Dore, J. H. Augustson, C. Hermanrud, D. J. Stewart, and O. Sylta, eds., Basin modeling: Advances and applications: Amsterdam, Elsevier, v. 3, p. 135–145.